Research Square

Preprints are preliminary reports that have not undergone peer review.
They should not be considered conclusive, used to inform clinical practice,
or referenced by the media as validated information.

Effect of Inclination Angle on Mixed Convective Heat Transfer in Bent Pipes

Aqsa Alamgir
National Textile University
Humayoun Shahid
National Textile University
sheheryar Mohsin Qureshi
sheheryar.qureshi@uws.ac.uk
University of the West of Scotland
Sadia Zahid
National Textile University
Muhammad Babar Ramzan
National Textile University

Article

Keywords: Flow analysis, Mixed convection, Heat transfer, Curved Pipe

Posted Date: November 12th, 2026

DOI: https://doi.org/10.21203/rs.3.rs-11391635/v1

License: This work is licensed under a Creative Commons Attribution 4.0 International License.
Read Full License

Additional Declarations: No competing interests reported.

Effect of Inclination Angle on Mixed Convective Heat Transfer in Bent Pipes

Aqsa Alamgir[1], Humayoun Shahid[1] Sheheryar Mohsin Qureshi*[2] Sadia Zahid[1]

Muhammad Babar Ramzan*[3]

[1]National Textile University Faisalabad, Faisalabad 38000, Pakistan

[2] Faculty of Computing, Sciences and Engineering University of the West of Scotland Paisley, Scotland, UK

[3]School of Engineering and Technology, National Textile University, Faisalabad, Punjab, Pakistan

*Corresponding author: sheheryar.qureshi@uws.ac.uk (SMQ); babar_ramzan@yahoo.com

Abstract

Mixed convection in bent pipes is of great interest in various engineering systems such as heat exchanger, cooling devices and fluid transport systems. Numerous investigations have been conducted in bent pipes with either flow or heat transfer, but the influence of pipe inclination and the combined effect of pipe inclination and mixed convection in bent pipe needs to be explored. The objective of this study is to examine the effect of Richardson number, Reynolds number, and the effect inclination angle on the flow and thermal behaviour of a bent pipe. The fundamental equations are non-dimensionalized and numerically solved in MATLAB by using the Finite Difference Method (FDM). Numerical analysis

are conducted different value of parameters, including Reynolds number ($200 \leq \mathrm{Re} \leq 2000$), Richardson number ($0.01 \leq \mathrm{Ri} \leq 10$) and inclination angle ($15^\circ \leq \phi \leq 75^\circ$). The results revealed that this convective transport mechanism is reinforced as the Reynolds number is increasing and the formation of vortices close to the bend region increases the heat transfer. The study offers valuable guidance for the design and optimization of bent-pipe systems.

Keywords: Flow analysis, Mixed convection, Heat transfer, Curved Pipe

1 Introduction

There are many engineering systems that are affected by heat transfer process, especially in thermal and fluid applications, and heat transfer is a fundamental transport process, which has a significant influence on the performance and efficiency of these systems Shahsavar et al. [1] The convective fluid flow and heat transfer in complex geometries like bent pipes with various inclination angles has been a significant topic of study in recent years, which is relevant to heat exchangers, cooling systems, and energy devices. Further development of heat transfer, with the aid of better thermal design and flow control, continues to be a key research objective. Numerous experimental studies have been conducted with respect to flow behavior and heat transfer mechanisms of engineering systems in either free Hickie-Bentzen et al. [2] or forced convection Lauriat, G., & Ghafir [3] conditions.

For complex pipe arrangements, fluid flow, thermal gradients and geometric factors are all important in determining the overall heat transfer performance. Curved pipes with different inclinations add further complication when considering the flow due to the curvature and buoyancy effects which affect velocity and temperature distribution. Thus, it is very important to understand these two coupled flows and thermal behavior for optimizing thermal systems. Numerical simulation techniques, especially

Computational Fluid Dynamics (CFD) are effective tools to study flow heat transfer characteristics and flow in the geometry and to gain in-depth knowledge of thermal performance of such geometries Carmeliet et.al [4]. The laminar flow of a periodically changing annulus was analyzed by A.T. Prata and E.M. Sparrow [5] and it was found that it considerably improved the heat transfer. Fully developed flow for heat transfer from S.V. Patankar, C.H. Liu, and E.M. Sparrow [6] were used for the isothermal plate segments creating a model of a heat exchanger. Laminar flow solution showed large recirculation areas and blockage. The developed Nusselt numbers were significantly greater than in a conventional laminar duct flow and were very sensitive to the Re.

The study of heat pipes carried out by M. A. Merrigan, E. S. Keddy at.al [7] at different angles showed that there are substantial differences in heat transfer mechanisms in all of the cases. They conclude that the optimization of the angles is crucial for improving thermal efficiency. Also, N. Acharya, M. Sen, and H.-C. Chang [8] carried out a numerical simulation of the heat transfer in 90° and 180° bends. They found that in the 180° bend, heat transfer was 6% to 8% better than for the 90° bend.

The laminar mixed convection of an inclined finned tube was numerically analyzed under the assumption of uniform solar flux. The effects of buoyancy-induced secondary flow were significant and enhanced heat transfer for both velocity and temperature distributions. The finned tube had a higher fully developed Nusselt number than the bare tube M. Ouzzane, and N. Galanis [9]. Laminar mixed convection of supercritical CO_2 in an inclined tube with constant wall temperature has been studied numerically. The results revealed that the greatest heat transfer occurred for horizontal flow with inclination angles of $\alpha = \pm 30°$ showing some improvement based on secondary flow effects. The effect of inclination was reduced when gravity force was less and a combination parameter was used to quantify the buoyancy effect Y. Chuanyong, X.Jinliang and W. Xiaodong [10]. The results indicate three flow regimes that occur as the cavity rotates from 0° to 360°: buoyancy-controlled flow, inertia-controlled flow, and a transition region between buoyancy and inertia dominant flows. Sometimes more than one circu-

lation cells develops, which improves heat transfer performance, resulting in oscillatory behavior of local Nusselt number and local friction factor L.Chin, and C.Yun [11].

C.Huajun, and Z.Benzhao [12] examined the combined influence of rotation, pipe curvature and thermal parameters for a huge range of parameters. The changes in the flow are studied and the effect on the flow pattern, distribution temperature, Nusselt number and friction factor are studied. The results obtained are useful to have a better understanding of the behavior of heat transfer and fluid flow in rotating curved pipes.

The laminar three-dimensional flow and transfer of heat in a channel that features inclined baffles mounted on opposite channel walls at an angle of 30° are numerically examined for periodic flow. The SIMPLE algorithm and the finite volume method is used from 100 to 2000 for Reynolds numbers. The inclined baffles generate a counter-rotating vortex in the flow direction, enhancing the mixing of the fluid and the alteration of the heat transfer in the channel is significantly increased. The results show that the optimum values of pitch ratio and baffle height give the maximum thermal enhancement factor, as found in C.Huajun, and Z.Benzhao [12].

The primary objective of this research is to carry out a simulation study on the mixed convective of fluid flow and heat transfer through a bent pipe with various inclined angles. The influence of Reynolds number, Richardson number and inclination angle on the characteristics of flow structures, temperature distribution and heat transfer is studied. The objective of this research is to improve the thermal performance in engineering applications with curved geometry, where the forced and natural convection in the geometry should be balanced appropriately. For improving the efficiency of heat exchangers, cooling systems, and other thermal engineering devices, the results of this study provide important insights.

2 Mathematical Formulation

In this part, the curved pipe geometry and parameters of interest in the present numerical study are presented. The computational domain and flow conditions are outlined

to investigate the heat transfer of mixed convection under various inclination angles. The configuration is set to enable the simulation to accurately reflect flow and thermal characteristics in the curved pipe.

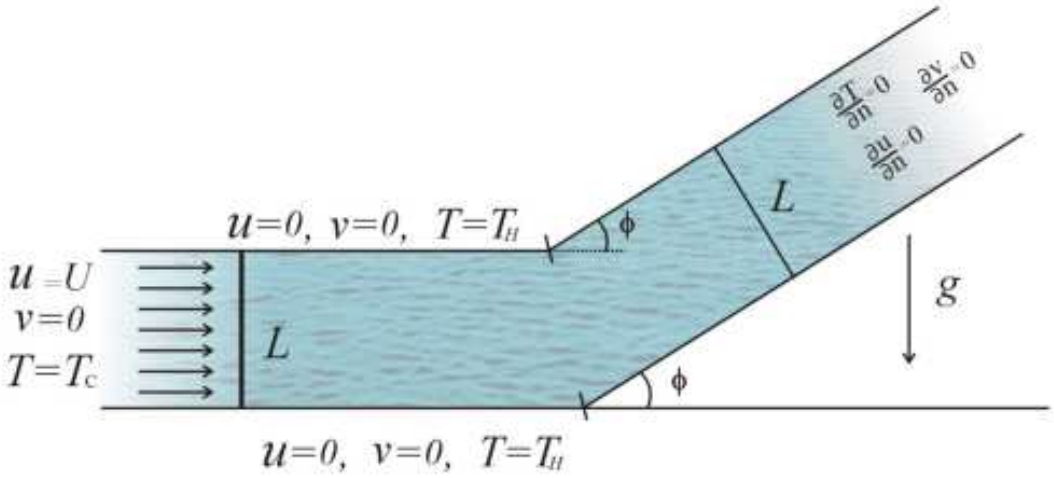


Figure 1: Mixed convective heat and fluid flow in curved pipe.

2.1 Physical Model

The computational domain is a two dimensional inclined channel geometry coupled with a horizontal inlet section as illustrated in Fig. 1. The dimensions of the horizontal part are L in height and the inclined part is L in length and inclined at an angle of ϕ. Cold fluid enters through the left inlet, where the boundary conditions are $u = U$, $v = 0$, and $T = T_C$. The flow leave through the inclined outlet where the thermally fully developed conditions, defined as $\frac{\partial u}{\partial n} = 0$, $\frac{\partial v}{\partial n} = 0$, and $\frac{\partial T}{\partial n} = 0$, where n denotes the outward direction normal at the outlet boundary. The lower horizontal wall and the lower inclined wall are preserved at a fixed hot temperature $T = T_H$ and satisfy the no-slip condition with $u = 0$ and $v = 0$. The upper inclined wall is considered adiabatic, for which $\frac{\partial T}{\partial n} = 0$. The gravitational acceleration g acts vertically downward and influences the flow through buoyancy effects.

2.2 Governing Equations

The overall momentum equation is defined as the following equation.

$$\frac{\partial u}{\partial x} + \frac{\partial v}{\partial y} = 0, \tag{1}$$

$$\frac{\partial u}{\partial t} + u\frac{\partial u}{\partial x} + v\frac{\partial u}{\partial y} = -\frac{1}{\rho}\frac{\partial P}{\partial x} + \nu\left(\frac{\partial^2 u}{\partial x^2} + \frac{\partial^2 u}{\partial y^2}\right), \tag{2}$$

$$\frac{\partial v}{\partial t} + u\frac{\partial v}{\partial x} + v\frac{\partial v}{\partial y} = -\frac{1}{\rho}\frac{\partial P}{\partial y} + \nu\left(\frac{\partial^2 v}{\partial x^2} + \frac{\partial^2 v}{\partial y^2}\right) + g\beta(T - T_o), \tag{3}$$

$$\frac{\partial T}{\partial t} + u\frac{\partial T}{\partial x} + v\frac{\partial T}{\partial y} = \alpha\left(\frac{\partial^2 T}{\partial x^2} + \frac{\partial^2 T}{\partial y^2}\right). \tag{4}$$

The continuity equation is given in Eq. (1) and the momentum equations in x and y directions are given in Eqs. (2) and (3) respectively while the energy equation is given in Eq. (4). The velocity of components u and v represent the motion of the fluid, and the pressure P is the driving force of the flow and g denotes gravitational acceleration, β is the thermal expansion coefficient, T is the local fluid temperature, and T_0 is the reference temperature. Inertial effects are controlled by density ρ and viscous effects are controlled by kinematic viscosity ν, α is the thermal diffusion parameter, it gives as $\alpha = \frac{k}{\rho C_p}$ where ρ is the density, C_p is the specific heat and k is the thermal conductivity and $\left(u\frac{\partial T}{\partial x} + v\frac{\partial T}{\partial y}\right)$ is heat flux. We now get all the equations in dimensionless.

$$u^* = \frac{u}{U}, \quad v^* = \frac{v}{U}, \quad x^* = \frac{x}{L}, \quad y^* = \frac{y}{L}, \quad t^* = \frac{tU}{L}, \quad P^* = \frac{P}{\rho U^2}, \tag{5}$$

$$\theta = \frac{T - T_0}{\Delta T} + \frac{1}{2}, \quad Ri = \frac{Gr}{Re^2}, \quad Re = \frac{UL}{\nu}, \quad Gr = \frac{g\beta\Delta T L^3}{\nu^2}. \tag{6}$$

The non-dimensional velocities are u^* and v^* while the non-dimensional coordinates are x^* and y^* and the non-dimensional time is t^*, here L is the characteristic length. The average temperature is $T_0 = \frac{T_H + T_C}{2}$, with T_H and T_C denoting hot upper wall temperature and cold inlet temperature, here the Grashof number is Gr where g is the gravitational acceleration, β is the thermal expansion coefficient, ΔT is the temperature

difference, L is the characteristic length, and ν is the kinematic viscosity. The reference velocity and length are U and L; ρ, u, v, x, y, t and P are the fluid density velocity, position, and pressure.

$$\frac{\partial u^*}{\partial x^*} + \frac{\partial v^*}{\partial y^*} = 0, \tag{7}$$

$$\frac{\partial u^*}{\partial t^*} + u^*\frac{\partial u^*}{\partial x^*} + v^*\frac{\partial u^*}{\partial y^*} = -\frac{\partial P^*}{\partial x^*} + \frac{1}{Re}\left(\frac{\partial^2 u^*}{\partial x^{*2}} + \frac{\partial^2 u^*}{\partial y^{*2}}\right), \tag{8}$$

$$\frac{\partial v^*}{\partial t^*} + u^*\frac{\partial v^*}{\partial x^*} + v^*\frac{\partial v^*}{\partial y^*} = -\frac{\partial P^*}{\partial y^*} + \frac{1}{Re}\left(\frac{\partial^2 v^*}{\partial x^{*2}} + \frac{\partial^2 v^*}{\partial y^{*2}}\right) + Ri\left(\theta - \frac{1}{2}\right), \tag{9}$$

$$\frac{\partial \theta}{\partial t^*} + u^*\frac{\partial \theta}{\partial x^*} + v^*\frac{\partial \theta}{\partial y^*} = \frac{1}{RePr}\left(\frac{\partial^2 \theta}{\partial x^{*2}} + \frac{\partial^2 \theta}{\partial y^{*2}}\right). \tag{10}$$

In this case Re and Pr are the Reynolds numbers, Prandtl numbers, respectively.

2.3 Vorticity-Sream Function

The vorticity-stream function formulation (VSFF) is used to convert the governing equations from primitive variables to stream function and vorticity variables. Taking the derivative of Eqs. (8) and (9) with respect to y and x respectively, gives

$$\frac{\partial}{\partial t}\left(\frac{\partial u}{\partial y}\right) + u\frac{\partial}{\partial x}\left(\frac{\partial u}{\partial y}\right) + v\frac{\partial}{\partial y}\left(\frac{\partial u}{\partial y}\right) = -\frac{\partial^2 P}{\partial x \partial y} + \frac{1}{Re}\left(\frac{\partial^2}{\partial x^2}\frac{\partial u}{\partial y} + \frac{\partial^2}{\partial y^2}\frac{\partial u}{\partial y}\right), \tag{11}$$

$$\frac{\partial}{\partial t}\left(\frac{\partial v}{\partial x}\right) + u\frac{\partial}{\partial x}\left(\frac{\partial v}{\partial x}\right) + v\frac{\partial}{\partial y}\left(\frac{\partial v}{\partial x}\right) = -\frac{\partial^2 P}{\partial x \partial y} + \frac{1}{Re}\left(\frac{\partial^2}{\partial x^2}\frac{\partial v}{\partial x} + \frac{\partial^2}{\partial y^2}\frac{\partial v}{\partial x}\right) + Ri\frac{\partial \theta}{\partial x}. \tag{12}$$

Subtracting Eq. (11) from Eq. (12) and from the definition of vorticity given in Eq. (14) the equation given as Eq. (13) is obtained.

$$\frac{\partial \omega}{\partial t} + u\frac{\partial \omega}{\partial x} + v\frac{\partial \omega}{\partial y} = \frac{1}{Re}\left(\frac{\partial^2 \omega}{\partial x^2} + \frac{\partial^2 \omega}{\partial y^2}\right) + Ri\frac{\partial \theta}{\partial x}, \tag{13}$$

$$\omega = \frac{\partial v}{\partial x} - \frac{\partial u}{\partial y}. \tag{14}$$

Using the stream function definitions $u = \frac{\partial \psi}{\partial y}$ and $v = -\frac{\partial \psi}{\partial x}$ in Eqs. (14) and (13). This convert our Navier-Stokes equations into a coupled system consisting of a Poisson equation and an advection–diffusion equation given by Eqs. (15) and (16). In a similar way, the energy equation can also be represented in terms of the stream function Eq. (17) is formed.

$$\omega = -\left(\frac{\partial^2 \psi}{\partial x^2} + \frac{\partial^2 \psi}{\partial y^2}\right), \tag{15}$$

$$\frac{\partial \omega}{\partial t} + \frac{\partial \psi}{\partial y}\frac{\partial \omega}{\partial x} - \frac{\partial \psi}{\partial x}\frac{\partial \omega}{\partial y} = \frac{1}{Re}\left(\frac{\partial^2 \omega}{\partial x^2} + \frac{\partial^2 \omega}{\partial y^2}\right) + Ri\frac{\partial \theta}{\partial x}, \tag{16}$$

$$\frac{\partial \theta}{\partial t} + \frac{\partial \psi}{\partial y}\frac{\partial \theta}{\partial x} - \frac{\partial \psi}{\partial x}\frac{\partial \theta}{\partial y} = \frac{1}{Re\,Pr}\left(\frac{\partial^2 \theta}{\partial x^2} + \frac{\partial^2 \theta}{\partial y^2}\right). \tag{17}$$

2.3.1 Governing Equations in Curvilinear Form

In the present study, an analytical grid generation method is used to convert the physical domain into a computational domain. The grid points are shown in terms of the computational coordinates (ξ, η), where the physical coordinates are given by:

$$x = x(\xi, \eta), \qquad y = y(\xi, \eta).$$

The variables in Eqs. (15), (16) and (17) are changed from the physical variables (x, y) to the computational variables (ξ, η) with the help of the chain rule. Let $f = f(x, y)$ be an arbitrary scalar quantity, where $x = x(\xi, \eta)$ and $y = y(\xi, \eta)$. Now, f can be computed in the computational domain as $\hat{f}(\xi, \eta)$. Then the desired derivatives in the changed coordinate system can be calculated by means of familiar chain rule relations.

$$q_1\psi_{\xi\xi} - 2q_2\psi_{\xi\eta} + q_3\psi_{\eta\eta} + J^2\nabla^2\xi\psi_\xi + J^2\nabla^2\eta\psi_\eta = -J^2\omega, \tag{18}$$

$$\frac{\partial\omega}{\partial t} + \frac{1}{J}\left(\omega_\xi\psi\eta - \psi_\xi\omega_\eta\right) = \frac{1}{ReJ^2}\left(q_1\omega_{\xi\xi} - 2q_2\omega_{\xi\eta} + q_3\omega_{\eta\eta} + J^2\nabla^2\xi\omega_\xi + J^2\nabla^2\eta\omega_\eta\right) + \frac{Ri}{J}\left(\theta_\xi y_\eta - \theta_\eta y_\xi\right), \tag{19}$$

$$\frac{\partial\theta}{\partial t} + \frac{1}{J}\left(\psi_\eta\theta_\xi - \psi_\xi\theta_\eta\right) = \frac{1}{RePrJ^2}\left(q_1\theta_{\xi\xi} - 2q_2\theta_{\xi\eta} + q_3\theta_{\eta\eta} + J^2\nabla^2\xi\theta_\xi + J^2\nabla^2\eta\theta_\eta\right). \tag{20}$$

The values of $q_1, q_2, q_3, \nabla^2\xi$ and $\nabla^2\eta$ are:

$$\nabla^2\xi = \frac{1}{J^3}\left(q_1\left(x_\eta y_{\xi\xi} - y_\eta x_{\xi\xi}\right) - 2q_2\left(x_\eta y_{\xi\eta} - y_\eta x_{\xi\eta}\right) + q_3\left(x_\eta y_{\eta\eta} - y_\eta x_{\eta\eta}\right)\right),$$

$$\nabla^2\eta = \frac{1}{J^3}\left(q_1\left(y_\xi x_{\xi\xi} - x_\xi y_{\xi\xi}\right) - 2q_2\left(y_\xi x_{\xi\eta} - x_\xi y_{\xi\eta}\right) + q_3\left(y_\xi x_{\eta\eta} - x_\xi y_{\eta\eta}\right)\right),$$

$$q_1 = x_\eta^2 + y_\eta^2, \quad q_2 = x_\xi x_\eta + y_\xi y_\eta, \quad q_3 = x_\xi^2 + y_\xi^2.$$

2.4 Analytical Grid Generation

The physical domain in the current study is converted into an appropriate computational domain using an analytical grid generation method. The appropriate physical coordinates are given by $x = x(\xi, \eta)$ and $y = y(\xi, \eta)$, whereas the grid points are represented in terms of the computational coordinates (ξ, η). A structured computational grid can reflect the curved geometry of the bent pipe thanks to the transformation, which creates a clear connection between the computational and physical domains. In order to accurately describe the geometry of the physical limits, the computational coordinates are chosen along the grid lines. This method distributes grid points across the computing domain in an orderly and continuous manner. The computational domain is specified in the curvilinear coordinates (ξ, η) where the discrete grid points along the ξ- and η-directions are denoted as M and N and its domain is given by $1 \leq \xi \leq M$

and $1 \leq \eta \leq N$. The indices are given by $i = 1, 2, 3, 4, \ldots, M$ implying $\xi_i = i$, and $j = 1, 2, 3, 4, \ldots, N$ implying $\eta_j = j$. The variables are then presented in the discrete form of:

$$x_{i,j} = x(\xi_i, \eta_j), \qquad y_{i,j} = y(\xi_i, \eta_j).$$

For the present computation, the grid size is taken as:

$$(M, N) = (513, 33).$$

The coordinate functions $x(\xi, \eta)$ and $y(\xi, \eta)$ are determined on all boundary edges of the computational domain. The boundary conditions are designated as:

$$(x(1, \eta),\, y(1, \eta)) = E_1, \qquad (x(M, \eta),\, y(M, \eta)) = E_2,$$

$$(x(\xi, 1),\, y(\xi, 1)) = E_3, \qquad (x(\xi, N),\, y(\xi, N)) = E_4.$$

In this case E_1, E_2, E_3, and E_4 are the four edges of the real geometry M and N is the set of the discretized points for the ξ and η axis. The interior points of the grid are then generated analytically over the computational domain after defining the boundary points.

The grid points are at the inside are represented by the coordinates of

$$x(\xi_i, \eta_j) = x_{i,j} = x_{i,1}$$

and

$$y(\xi_i, \eta_j) = y_{i,j} = y_{i,1} + \frac{(y_{i,N} - y_{i,1})j}{N - 1},$$

where x_{ij} and y_{ij} represent the physical coordinates of each grid node.

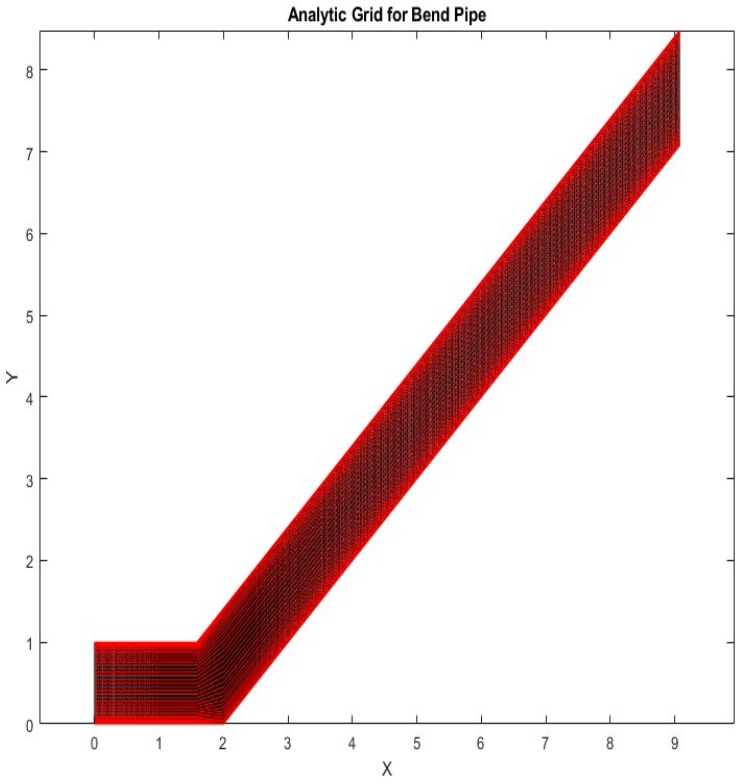


Figure 2: Generated Grid using Analytic Grid Generation with $(M, N) = (513, 33)$.

Bent pipe is a type of piping that has a horizontal section of pipe joined to an inclined section above. This geometry is used to study the effects of the bend and inclination on fluid flow and heat transfer characteristics. The block method is applied to create computational grid and MATLAB software is used to build and draw the computational grid which can be shown in Fig. 2. Firstly, the boundary points are determined based on the geometry of the bent pipe. The next step is to use the analytical grid formulation to compute the interior grid points within the boundaries specified. To obtain a suitable representation of the curved and inclined regions, the grid points are distributed systematically to conform to the shape of the physical domain. This results in a regular, organised and continuous mesh throughout the computational domain.

2.5 Numerical Method and Boundary Conditions

The boundary conditions corresponding to Fig. 1 are expressed in the form ψ, ω, and θ variables. The boundary conditions for ψ, θ, ω have been updated, following the method outlined in J. Chen, P. Yu et.al [13] and taking a volumetric flow rate of 1.

It is found that for second order accuracy careful treatment is required of the boundary conditions for ω that include derivatives. The method explained in J. Chen, P. Yu et.al [13] is used in order to achieve second order accuracy. The governing equations are spatially discretized by a second order finite difference scheme. The implicit part of the IMEX method is stable in this work, and the explicit part is stable for high Reynolds numbers (e.g. $Re = 1000$) without violating the CFL condition. This method is suitable for computation with a very fine grid spacing at walls and a manageable time step.

The semi-discrete system can be written as:

$$\frac{du}{dt} = f(u) + \lambda g(u), \tag{21}$$

here $f(u)$ denotes the nonlinear advection term, and $\lambda g(u)$ denotes the linear diffusion term (where λ is sometimes a scaling factor).

Table 1: Boundary Conditions for ω, ψ and θ.

Region	ψ	ω	θ
Inlet	$\psi(\xi,1) = \dfrac{\xi}{M}$	$\omega(\xi,1) = 6\left(1 - 2\dfrac{\xi}{M}\right)$	$\theta(\xi,1) = 1$
Outlet	$\left.\dfrac{\partial\psi}{\partial\xi}\right\|_{\xi=M} = 0$	$\left.\dfrac{\partial\omega}{\partial\xi}\right\|_{\xi=M} = 0$	$\left.\dfrac{\partial\theta}{\partial\xi}\right\|_{\xi=M} = 0$
Lower wall	$\psi(1,\eta) = 0$	$\omega(1,\eta) = -\left.\dfrac{q_1}{J^2}\dfrac{\partial^2\psi}{\partial\xi^2}\right\|_{\xi=1}$	$\theta(1,\eta) = 1$
Upper wall	$\psi(M,\eta) = 1$	$\omega(M,\eta) = -\left.\dfrac{q_1}{J^2}\dfrac{\partial^2\psi}{\partial\xi^2}\right\|_{\xi=M}$	$\theta(M,\eta) = 1$

The second order of accuracy, to be applied on conditions of ω that involve derivatives, is made use of by the method from Chen J, Yu P et.al [14]. The advection-diffusion equation is solved using second-order Implicit-Explicit (IMEX) method for time-discretization. Which is given as:

$$\begin{aligned}\frac{1}{\Delta t}\left[\left(\gamma+\frac{1}{2}\right)u^{n+1}-2\gamma u^{n}+\left(\gamma-\frac{1}{2}\right)u^{n-1}\right]&=(\gamma+1)f(u^{n})-\gamma f(u^{n-1})\\&+\nu\left[\left(\gamma+\frac{c}{2}\right)g(u^{n+1})+(1-\gamma-c)g(u^{n})+\frac{c}{2}g(u^{n-1})\right].\end{aligned}\tag{22}$$

2.6 Nusselt Number

The Nusselt number Nu is a dimensionless number that compares the convective heat transfer to the conductive heat transfer at a surface, given as:

$$Nu=\frac{hL}{k}.\tag{23}$$

Nu is the heat transfer, which is usually specified by the characteristic length L, the thermal conductivity k and the convective heat transfer coefficient h. It is a ratio of the significance of convection to conduction. The local Nusselt number at the top (or bottom) wall is given by:

$$Nu_{local}=-\frac{L}{\Delta T}\frac{\partial T}{\partial n}.\tag{24}$$

The unit normal vector is denoted by n. Local value along a surface is integrated to obtain the mean Nusselt number.

$$Nu_{avg}=\frac{1}{L}\int_{C}Nu_{local}\,ds.\tag{25}$$

Length of wall(s) L and averaging curve of the area C.

2.7 Numerical Validity

A case of a horizontal pipe is used for the validation of the numerical method which can be simplified to the standard Poiseuille flow though the parallel plates. As a comparison, the axial velocity is determined using its analytical solution.

$$u = 6u_0 \frac{y}{L}(1 - \frac{y}{L}).$$

We obtain the numerical solution by our method, which is very close to the exact solution, as displayed in Fig. 3. The mathematical modeling and the simulation were done by computer simulation through MATLAB. The experimental data of the bent channel ($\phi = 70°$ and $Re = 391$) are compared with those of Matsumoto, D. et.al [15]. It is obvious from Fig. 4 that the method developed in this research gives satisfactory results compared to the results reported by Matsumoto, D. et.al [15]. The numerical results are also compared with those from Nithiarasu, P., et.al [16] for a porous square enclosure, to validate the results.

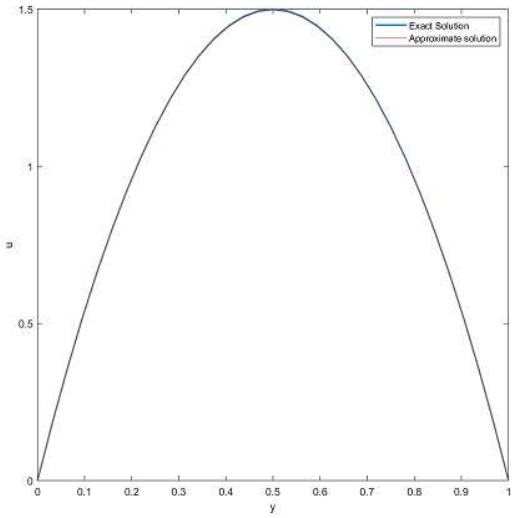
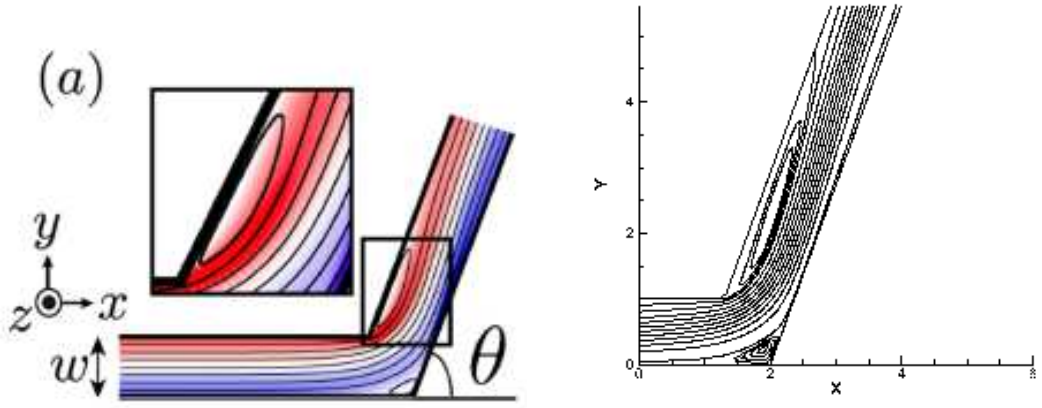


Figure 3: Comparison between the numerical approximation and exact solution.



(a) **(b)**

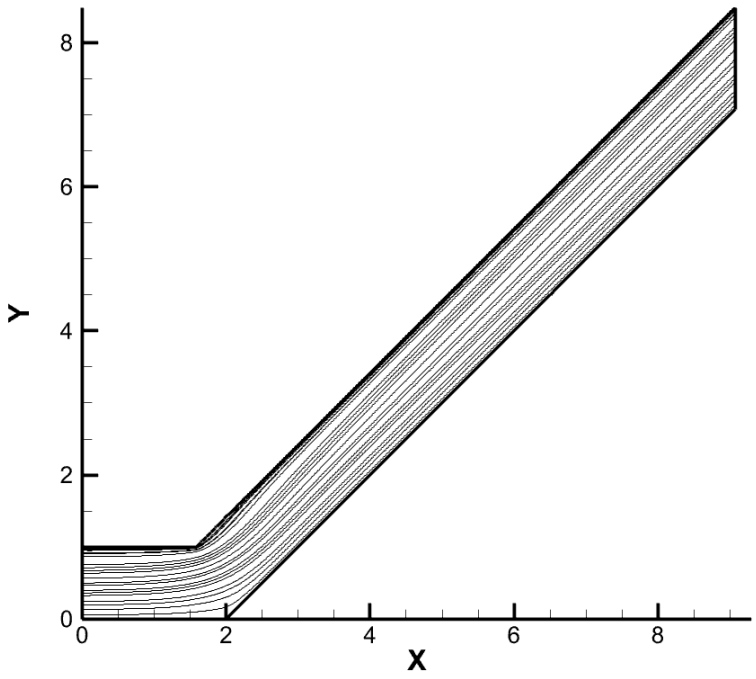
Figure 4: Comparison of the results with reference [15] for $Re = 391$ and $\phi = 70°$.

3 Results and Discussion

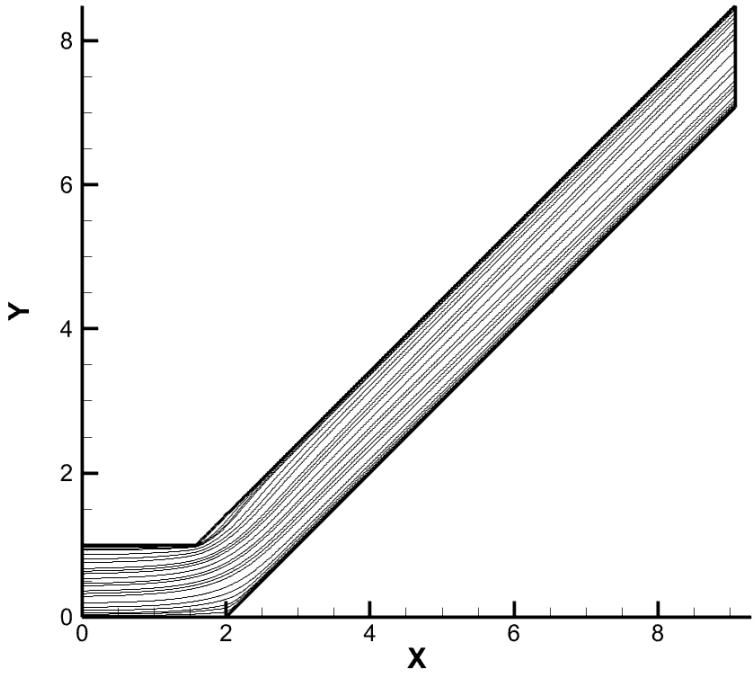
The velocity and temperature distribution within the curved pipe is a result of forced convection and natural convection. The natural convection is enhanced by the buoyancy force produced by the temperature difference and the imposed flow velocity forces the forced convection. The influence of these buoyancy effects can be greatly modified by the inclination angle, which results in modifications of the velocity and temperature fields over the domain. Appropriate inlet and outlet lengths are used to ensure the hydrodynamic and thermal conditions are well developed in the pipe for obtaining accurate and stable numerical solutions. The effects of Reynolds number, Richardson number and inclination angle on the flow structure and heat transfer efficiency are determined by numerical simulation on different values of these parameters.

In Fig. 5 the streamline at various Reynolds number $Re = 200$ to $Re = 2000$ are shown for a fixed Richardson number ($Ri = 1$) and inclination angle ($\phi = 45°$). For $Re = 200$ (Fig. 5a) the separation is not evident and the flow is mostly smooth with parallel streamlines and without any noticeable vortices due to the strong viscous forces which prevent separation. For $Re = 400$ (Fig. 5b), a small bending of the streamlines

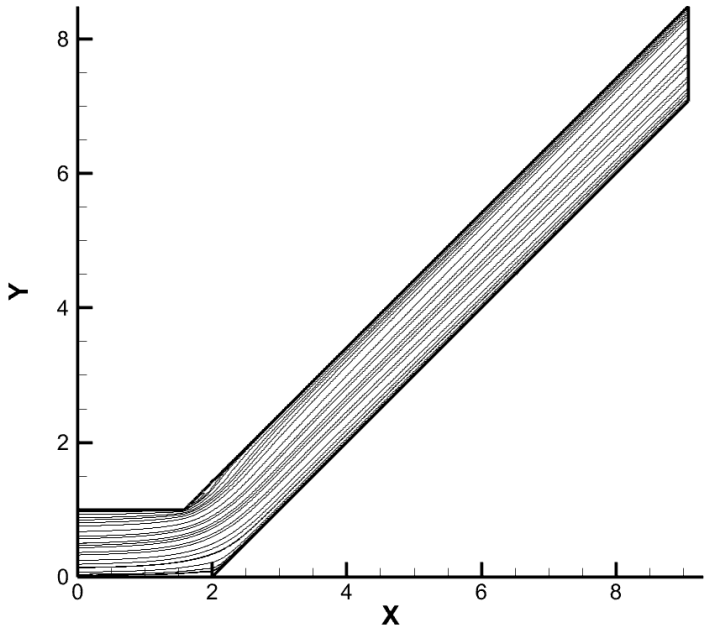
is observed near the bend, where the inertial effects are greater, but there is no vortex formation. When the Reynolds number is $Re = 600$, in Fig. 5c the flow is faster and there is more streamline compression and flow disturbance in the vicinity of the bend, but there is no distinct vortex observed. When the flow is mostly attached, the combined action of inertia, curvature and buoyancy at $Ri = 1$ produce weak swirling near the bend at $Re = 800$ (Fig. 5d). The flow is more unstable and separates locally, as seen in the increased recirculation region near the bend, at $Re = 1500$ (Fig. 5e). Inertial effects are more important at $Re = 2000$ (Fig. 5f), as they further promote flow separation and form a clear vortex near the bend. In summary, as the value of Re increases, the inertial forces grow and gradually favor flow separation and vortex generation in the bend region.



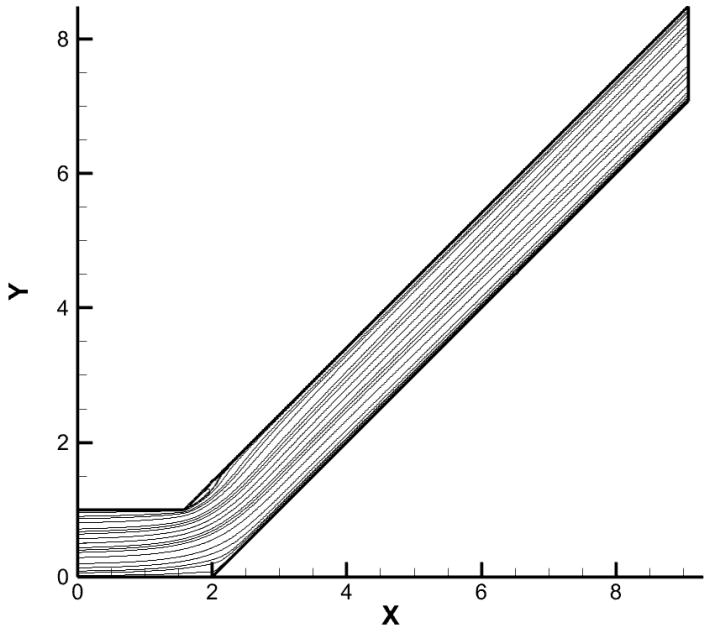
(a) Streamline at $Re = 200$



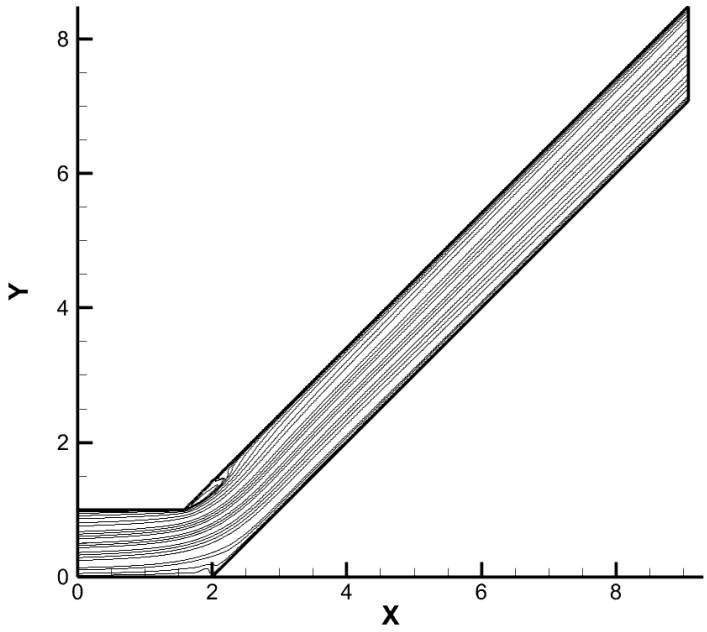
(b) Streamline at $Re = 400$



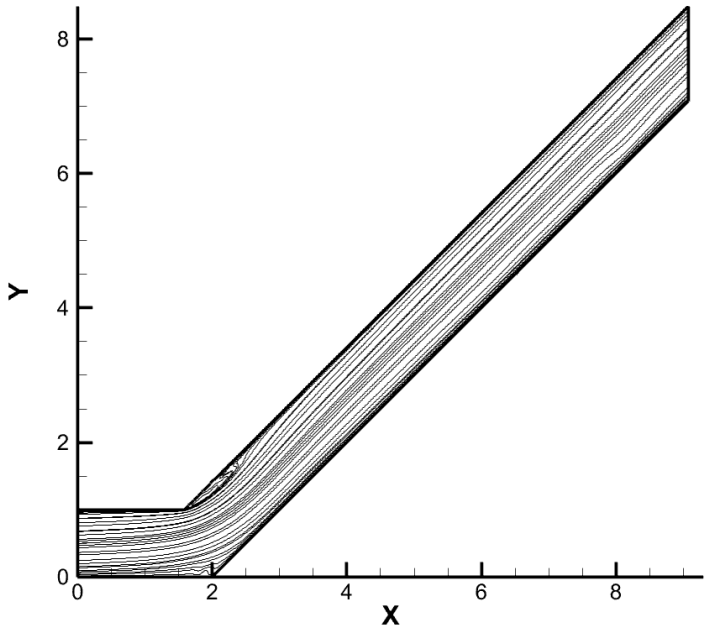
(c) Streamline at $Re = 600$



(d) Streamline at $Re = 800$



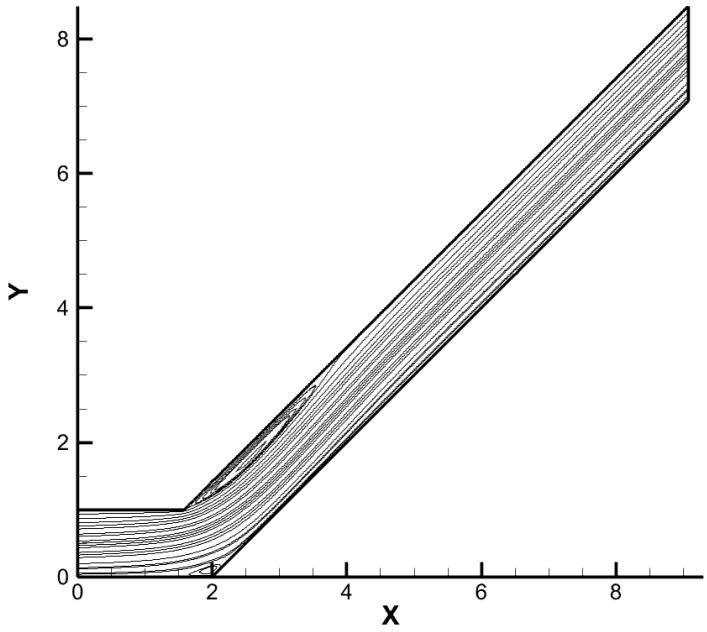
(e) Streamline at $Re = 1500$



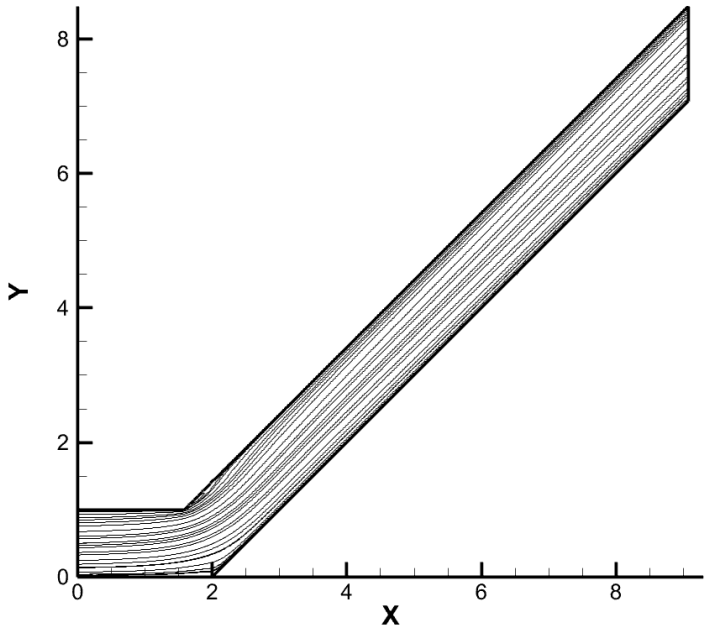
(f) Streamline at $Re = 2000$

Figure 5: Streamline for varying Re at $Ri = 1$ and $\phi = 45°$.

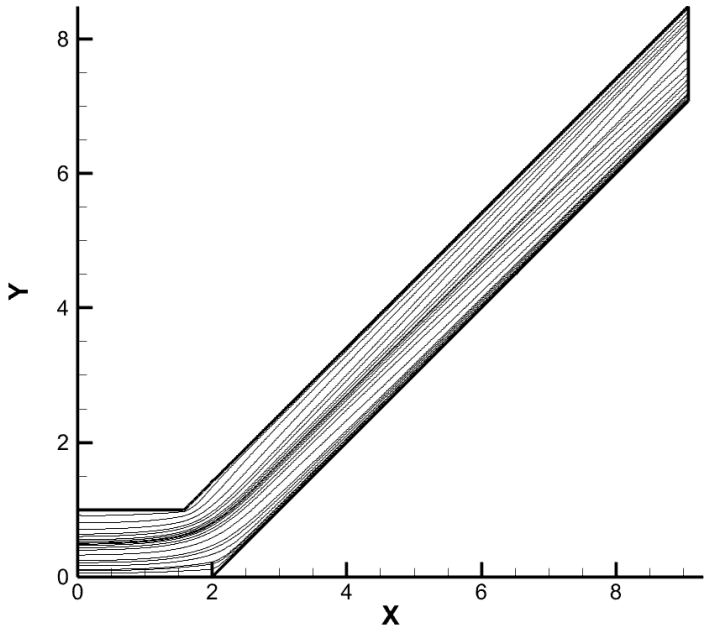
The streamlines at $Re = 600$ and $\phi = 45°$ with varying Richardson number $Ri = 0.01$ to 10 are shown in Fig. 6. Forced convection dominates at $Ri = 0.01$ (Fig. 6a) where a small recirculation region is seen near the bend where the flow direction changes and the pressure gradient is adverse. The inclination of the streamlines along the inclined section of the flow gradually increases as $Ri = 1$ (Fig. 6b) and $Ri = 3$ (Fig. 6c), but the flow remains mostly attached. As buoyancy increases at $Ri = 5$ (Fig. 6d), the streamlines are more distorted and the secondary flow is more prominent near the region of the bend. However, when $Ri = 10$ (Fig. 6e), the buoyancy has a strong effect on the flow and significant distortion of the streamlines is observed, as well as an increase in secondary circulation along the inclined section. In general, increasing Ri corresponds to a stronger relative buoyancy effect, associated with an increase in Gr or a reduction in Re, which gradually alters the flow structure, especially near the bend and along the inclined portion.



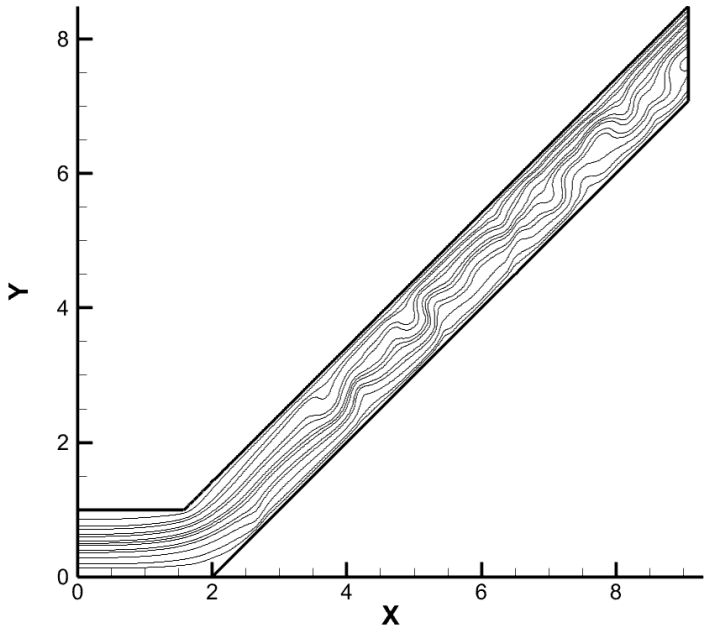
(a) Streamline at $Ri = 0.01$



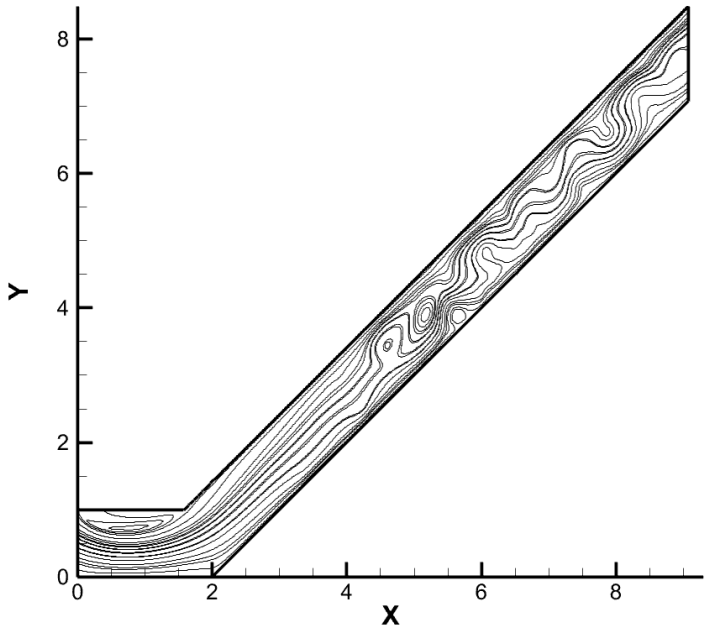
(b) Streamline at $Ri = 1$



(c) Streamline at $Ri = 3$



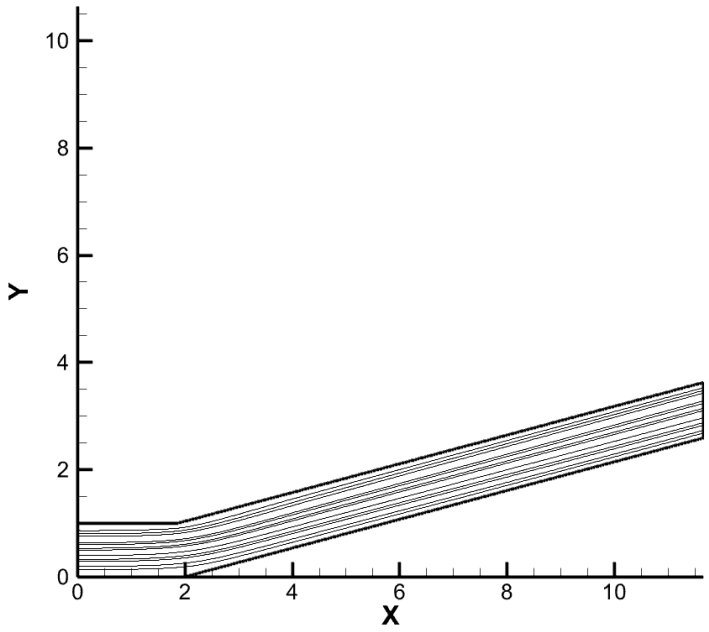
(d) Streamline at $Ri = 5$



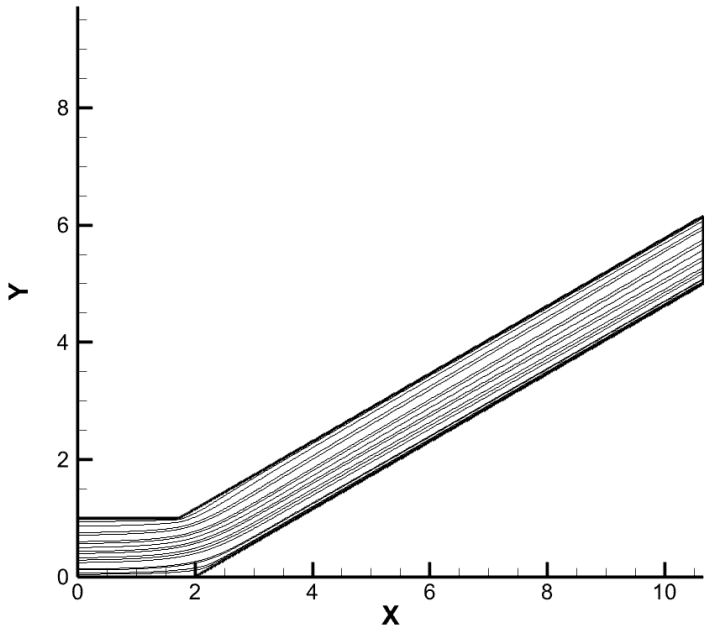
(e) Streamline at $Ri = 10$

Figure 6: Streamline for varying Ri at $Re = 600$ and $\phi = 45°$.

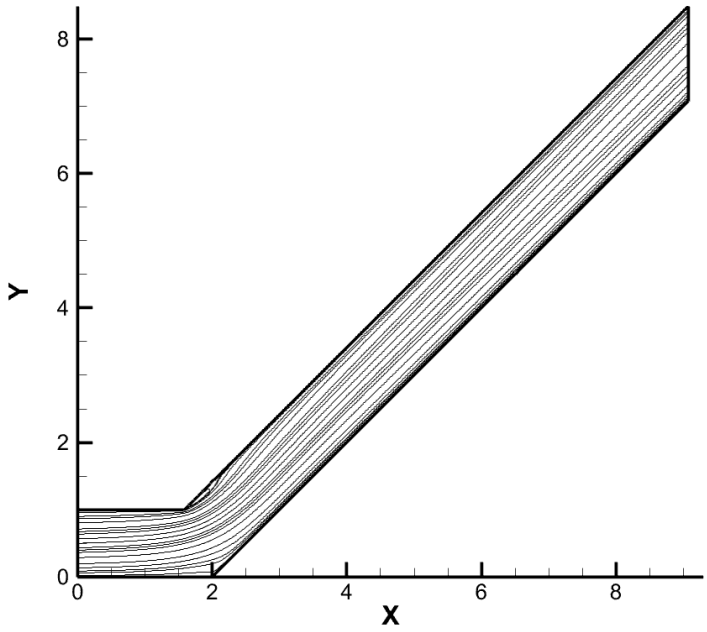
The streamlines at $Re = 800$ and $Ri = 1$ for various inclination angles $\phi = 15°$–$75°$ are shown in Fig. 7. As the value of the incline angle gets larger, the component of gravity in the direction of the pipe will get larger which will increase the buoyancy driven flow. The weak gravitational component along the pipe causes the streamlines to be almost parallel at a value of $\phi = 15°$ (Fig. 7a). The streamlines become increasingly inclined as the buoyancy effects increase at $\phi = 30°$ (Fig. 7b) and $\phi = 45°$ (Fig. 7c). Stronger buoyancy and inertial interactions close to the bend at $\phi = 60°$ and $75°$ (Figs. 7d and7e) result in the formation of recirculation zones. An increase in the inclination angle will these vortices also increases, which suggests that as the increases inclination angle, the interaction between the flow and the buoyancy forces increases.



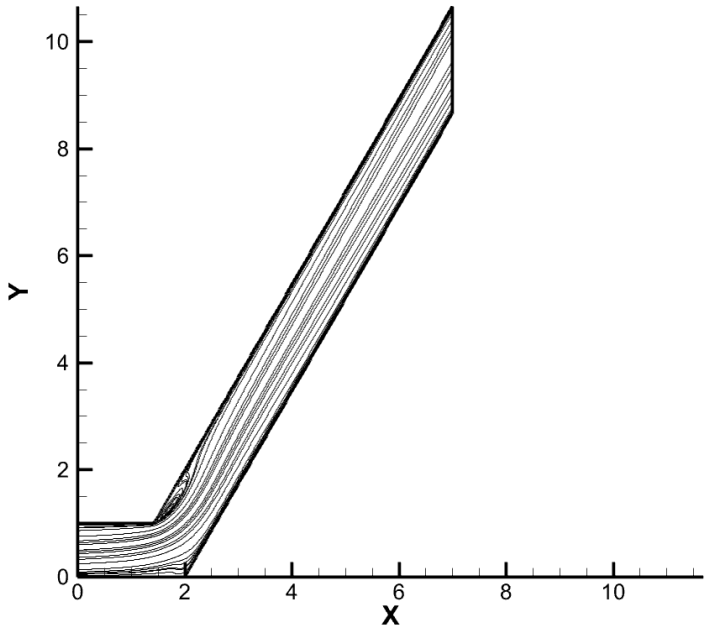
(a) Streamline at $\phi = 15°$



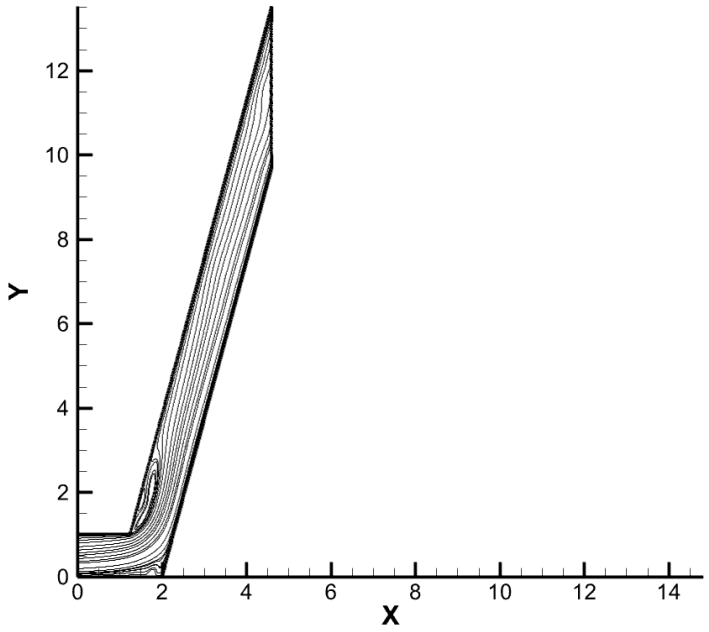
(b) Streamline at $\phi = 30°$



(c) Streamline at $\phi = 45°$



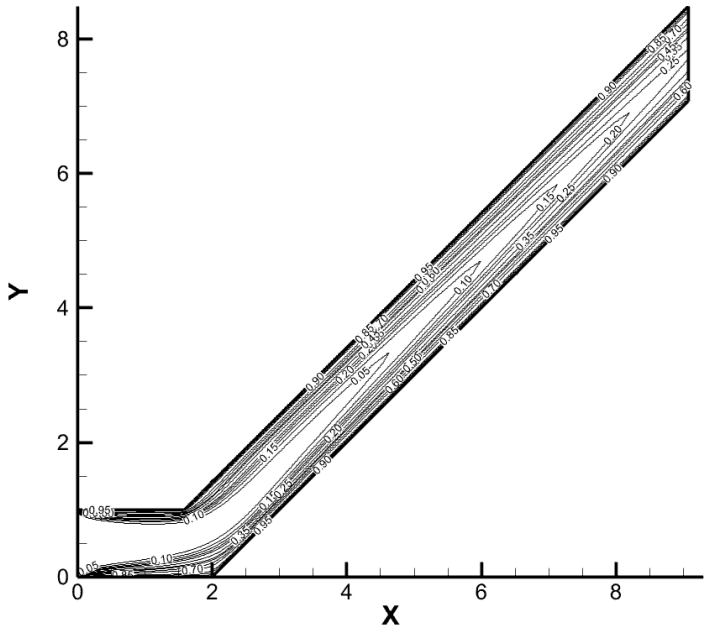
(d) Streamline at $\phi = 60°$



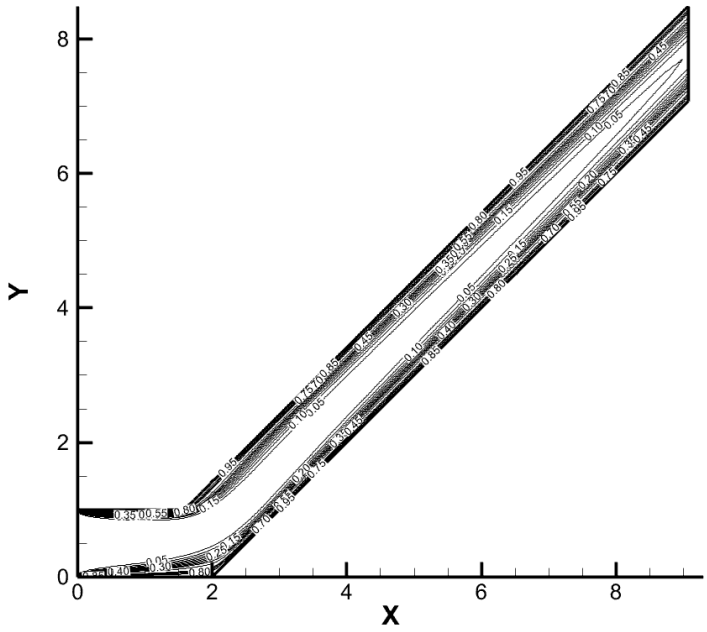
(e) $\phi = 75°$

Figure 7: Streamline for varying ϕ at $Re = 800$ and $Ri = 1$.

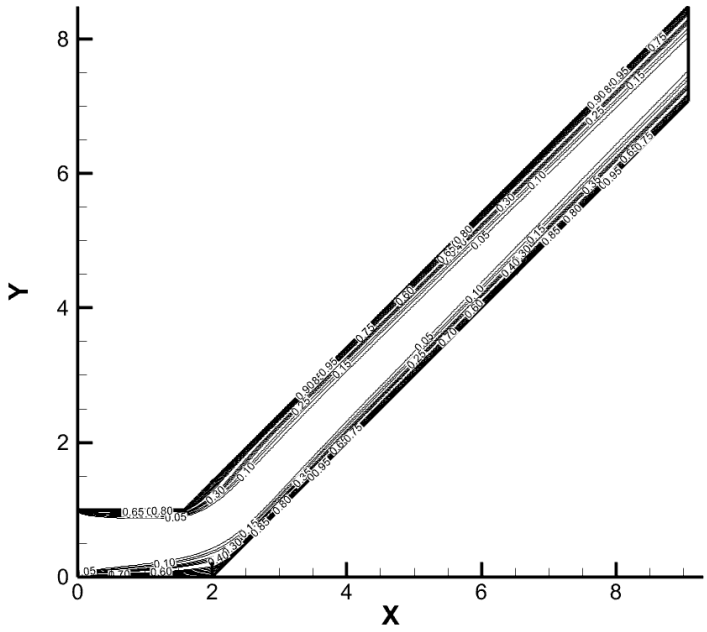
The isotherm for $Re = 200$–2000 at $Ri = 1$ and $\phi = 45°$ are shown in Fig. 8. For $Re = 200$ (Fig. 8a) the isotherms are very curved due to the low flow velocity, which makes thermal diffusion more important for the temperature field. The isotherms are elongated in the direction of the flow as Re is increased to 400 and 600 (Figs. 8b and 8c). As Re increases, the isotherms smoothen, become more elongated, and develop thicker thermal boundary layers at $Re = 800$ (Fig. 8d); at $Re = 1500$ and 2000 (Figs. 8e and 8f) the strong convection results in a thinner thermal boundary and increased convective transport of heat downstream. Hence, as Re is slowly increased, the heat transfer from the diffusion dominated to the convection dominated behavior is gradually shifted.



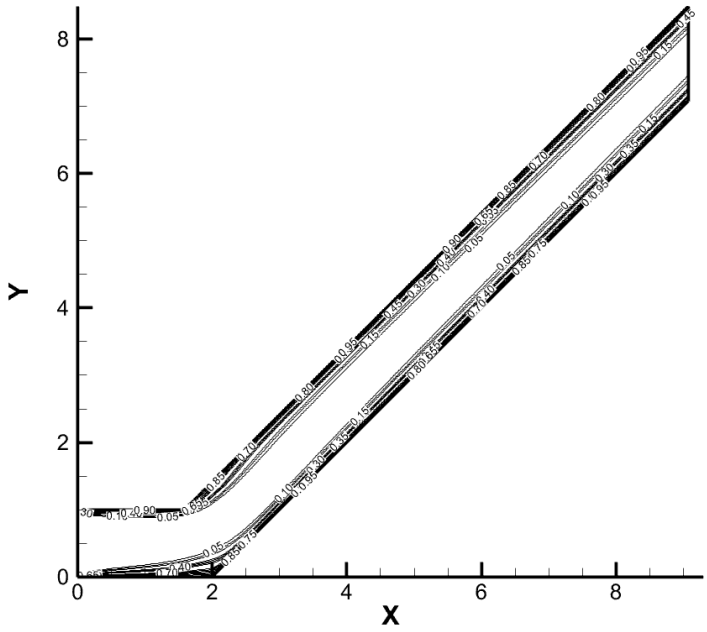
(a) Isotherm at $Re = 200$



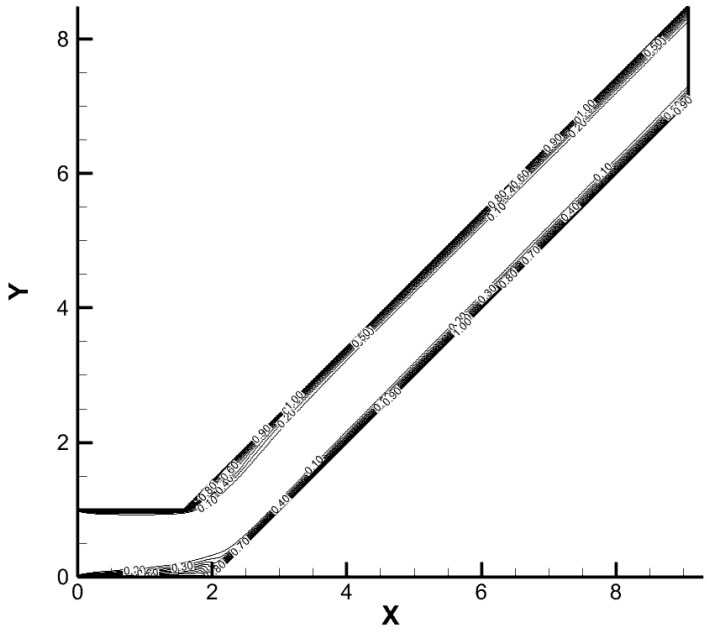
(b) Isotherm at $Re = 400$



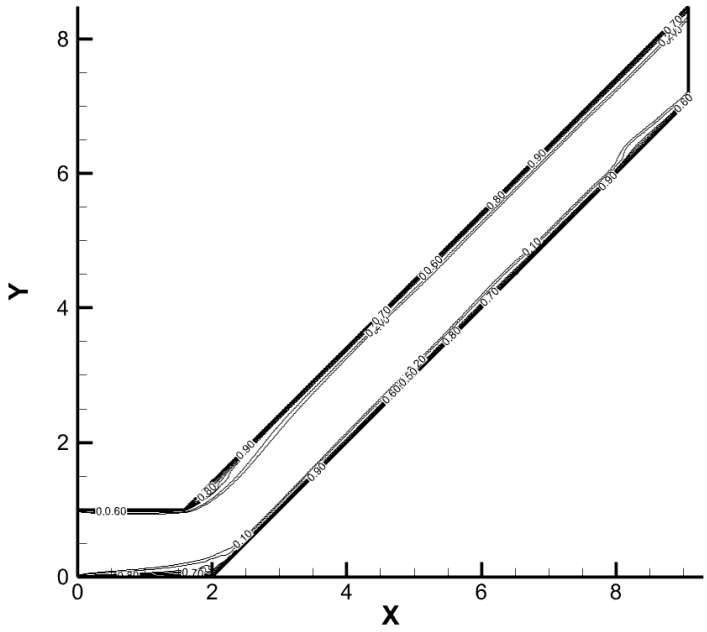
(c) Isotherm at $Re = 600$



(d) Isotherm at $Re = 800$



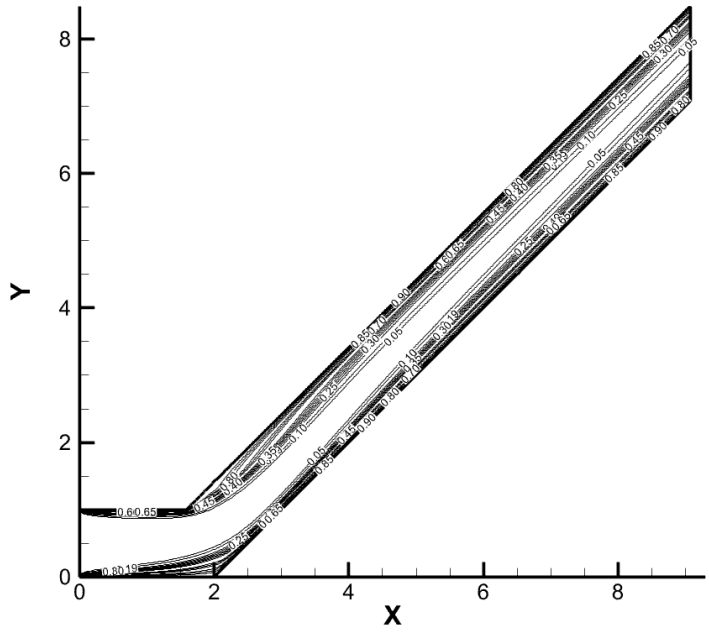
(e) $Re = 1500$



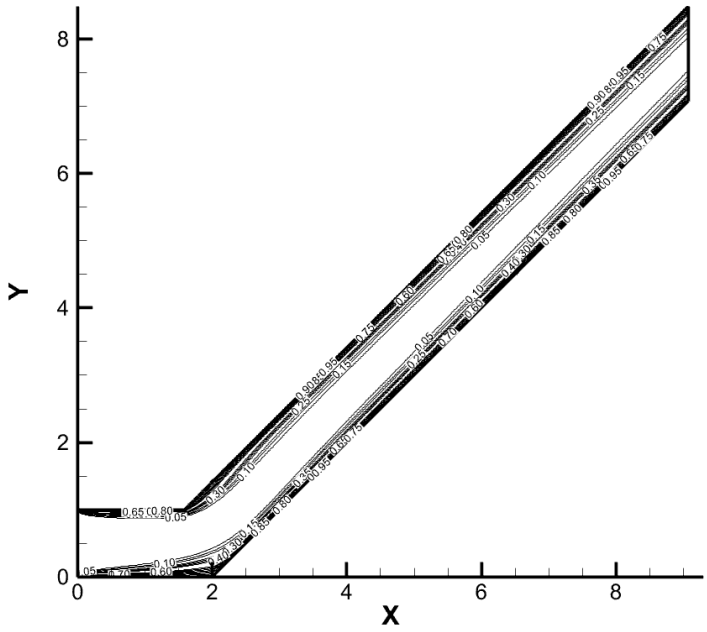
(f) Isotherm at $Re = 2000$

Figure 8: Isotherms for varying Re at $Ri = 1$ and $\phi = 45°$.

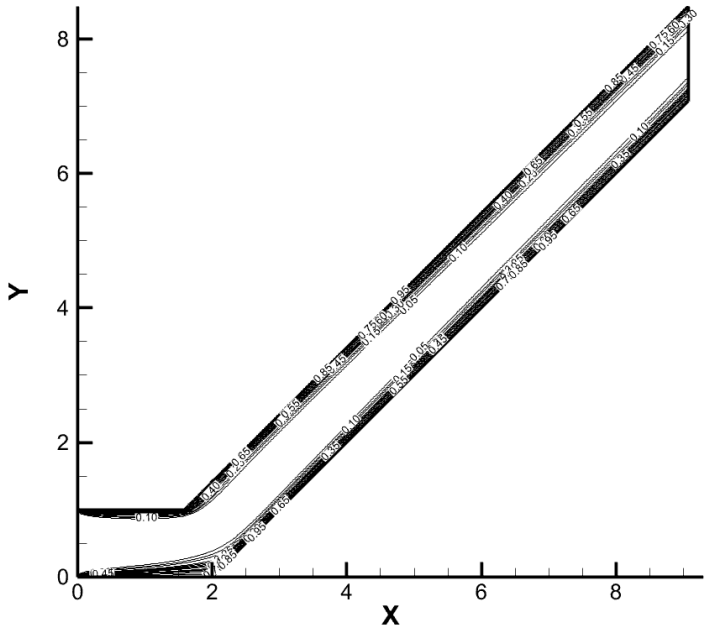
The isotherm for different Richardson numbers Ri are shown in Fig. 9 for $Re = 600$ and an inclination angle of $\phi = 45°$. For $Ri = 0.01$ (Fig. 9a) the forced convection is dominant, the isotherms are almost straight and parallel. This is because the buoyancy force is not strong enough to have a significant effect on the flow. As Ri increases from 1 (Fig. 9b), the isotherms begin to curve slightly, indicative of moderate thermal mixing, due to the influence of buoyancy on the flow. The isotherms of $Ri = 3$ (Fig. 9c) have a higher degree of curvature because the buoyancy force is higher and this increases the convective heat transfer. For $Ri = 5$ (Fig. 9d), the isotherms are further distorted due to increased buoyancy which causes secondary flow and recirculation which result in better thermal mixing. Natural convection is dominant and highly irregular isotherms are seen for $Ri = 10$ (Fig. 9e). The buoyancy induced circulation is strong, leading to strong mixing and heat transfer.



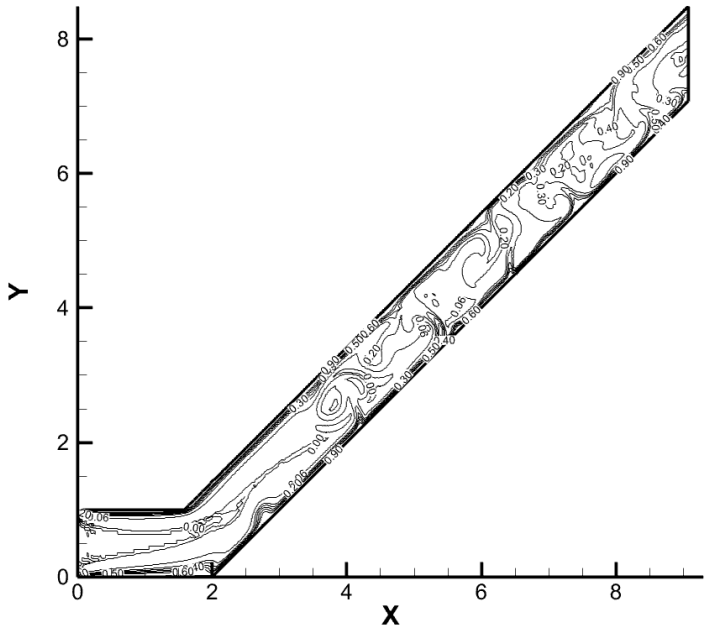
(a) Isotherm at $Ri = 0.01$



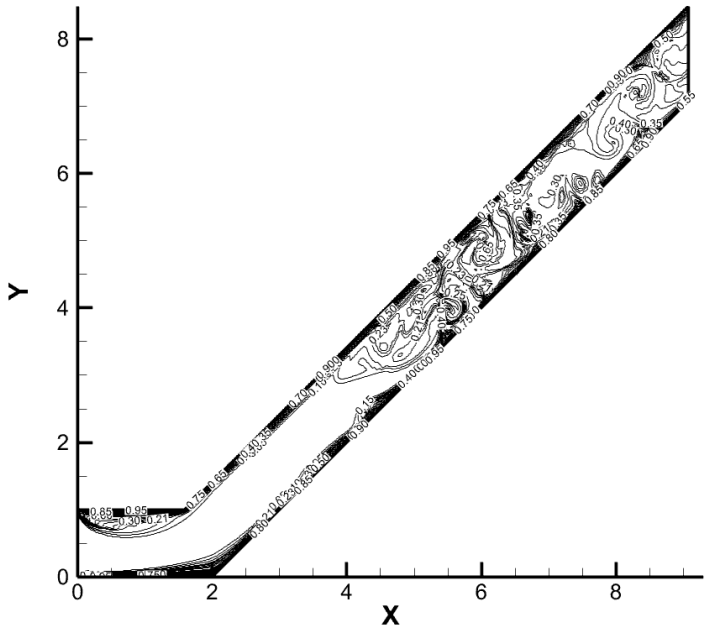
(b) Isotherm at $Ri = 1$



(c) Isotherm at $Ri = 3$



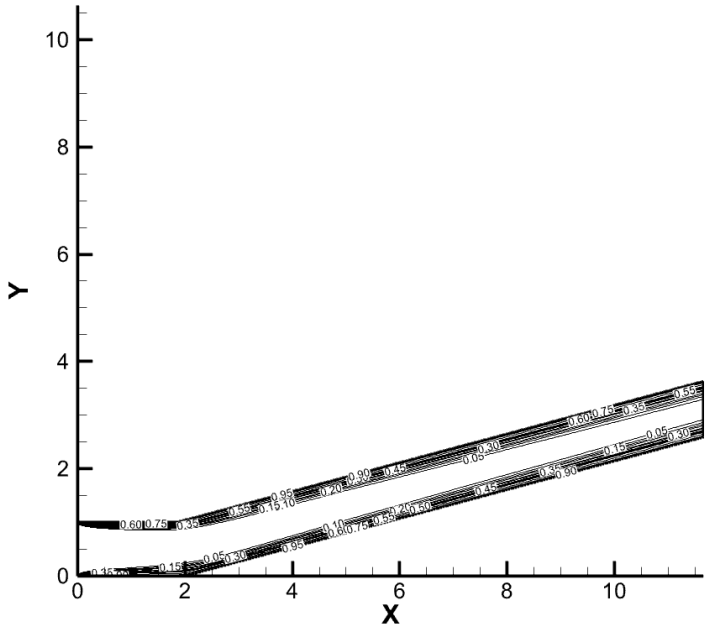
(d) Isotherm at $Ri = 5$



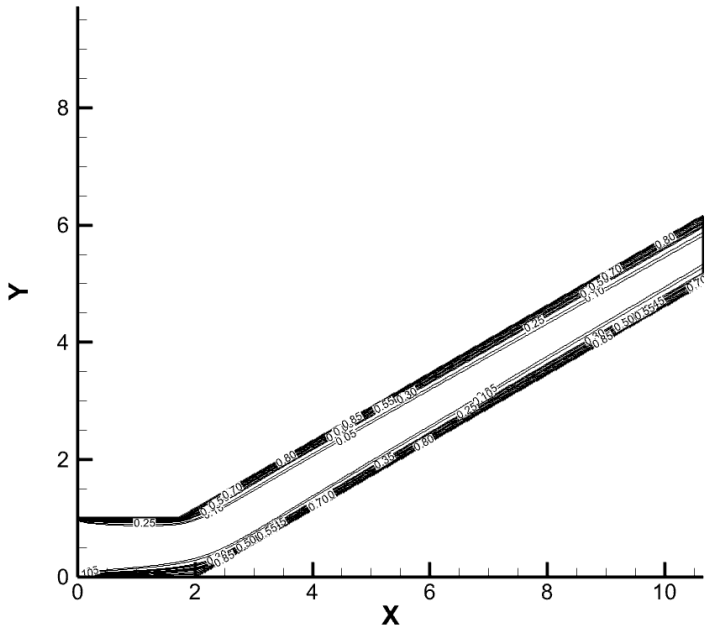
(e) Isotherm $Ri = 10$

Figure 9: Isotherms for varying Ri at $Re = 600$ and $\phi = 45°$.

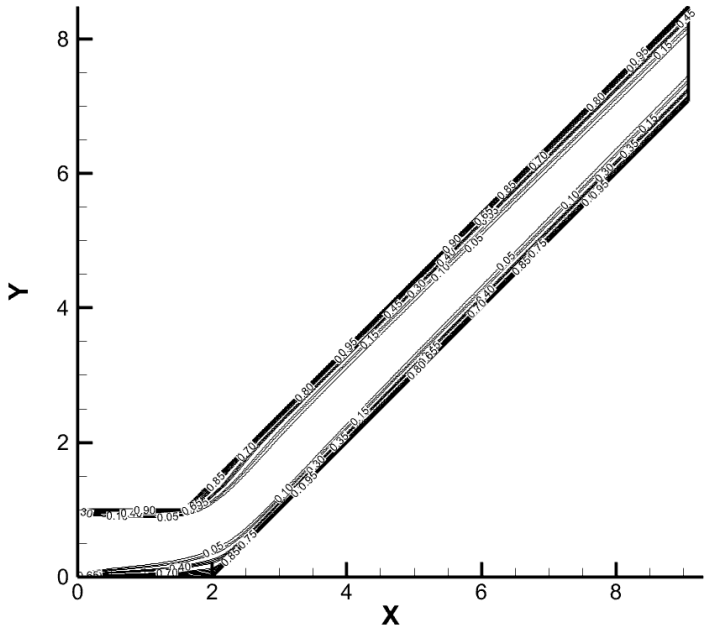
Isotherm plots of various inclinations ϕ at $Re = 800$ and $Ri = 1$ are presented in Fig. 10. The buoyancy is changed along the channel when changing the inclination angle, which will affect the temperature distribution. The isotherms are slightly curved, and mostly horizontal for $\phi = 15°$ (Fig. 10a) due to forced convection mode of heat transfer is the dominant mode of heat transfer because of the limited buoyancy contribution. When the buoyancy force increases, in this case, at $\phi = 30°$ (Fig. 10b), the isotherms turn upward, which increases convective heat transfer. In the case of $\phi = 45°$ (Fig. 10c), the isotherms are more inclined because of the influence of natural and forced convection, giving rise to enhanced thermal mixing. The isotherms are steeper and closer to the wall in the vicinity of the wall at $\phi = 60°$ (Fig. 10d), since the buoyancy affects the flow of heated fluid to be stronger and thus increases the flow rate. For the angle $\phi = 75°$ (Fig. 10e) the isotherms are almost vertical, and the channel is close to its vertical position, resulting in the natural convection as the dominant mode of heat transfer in the channel when the channel approaches the vertical position.



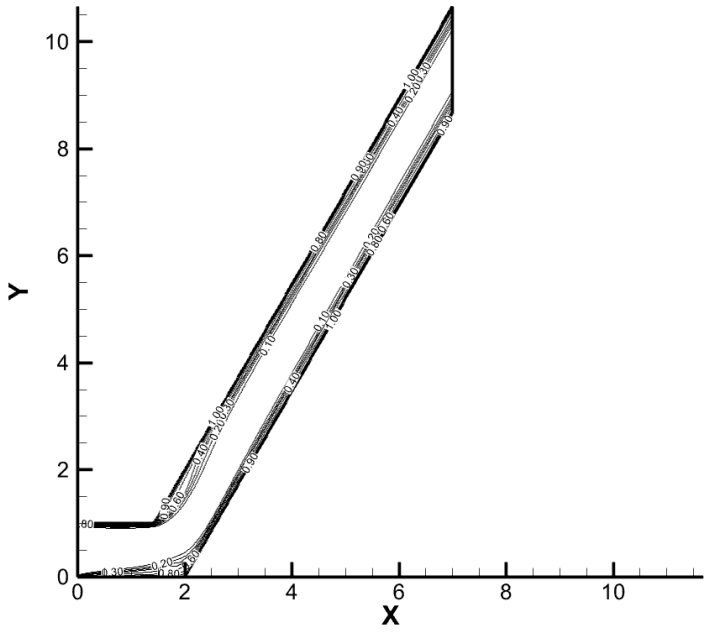
(a) Isotherm at $\phi = 15°$



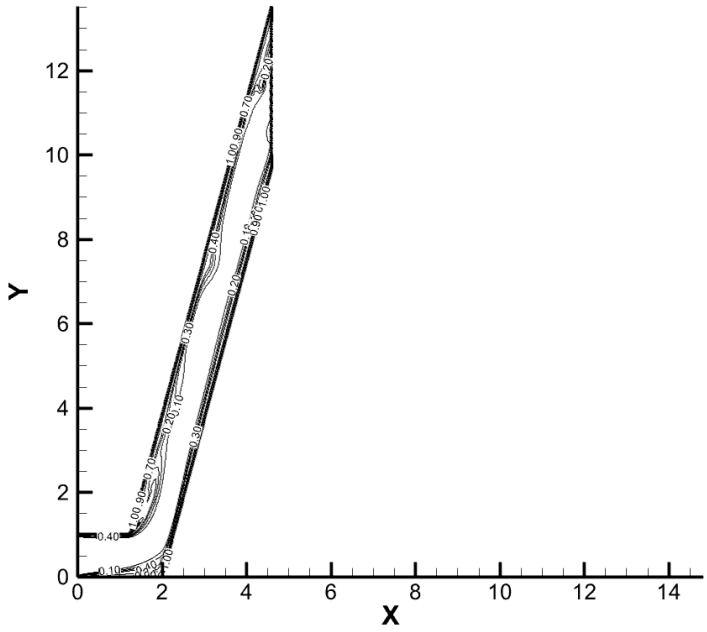
(b) $\phi = 30°$



(c) Isotherm at $\phi = 45°$



(d) Isotherm at $\phi = 60°$



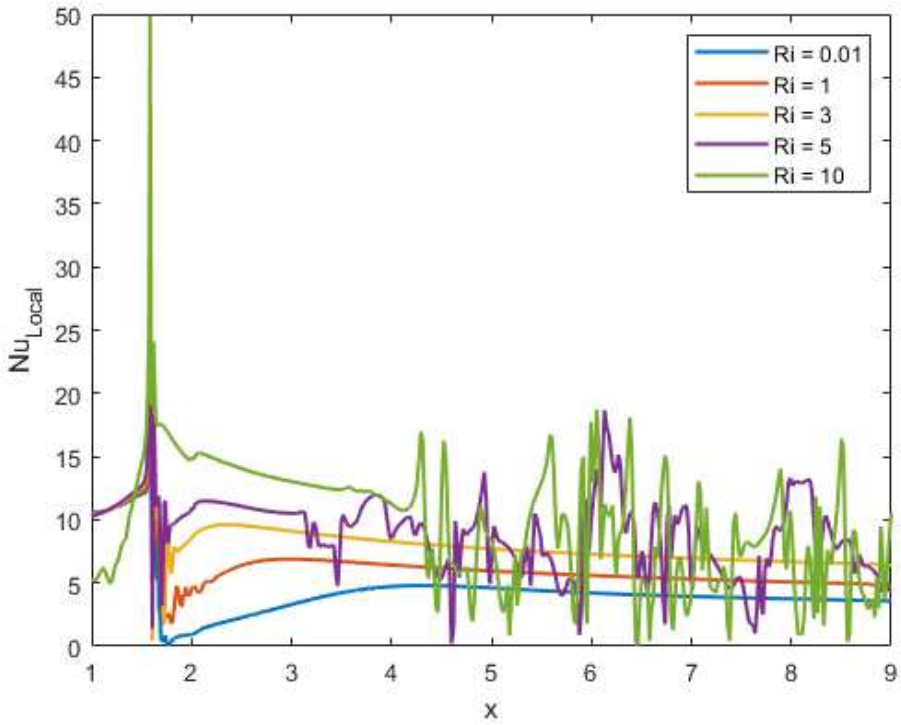
(e) Isotherm at $\phi = 75°$

Figure 10: Isotherms for varying ϕ at $Re = 800$ and $Ri = 1$.

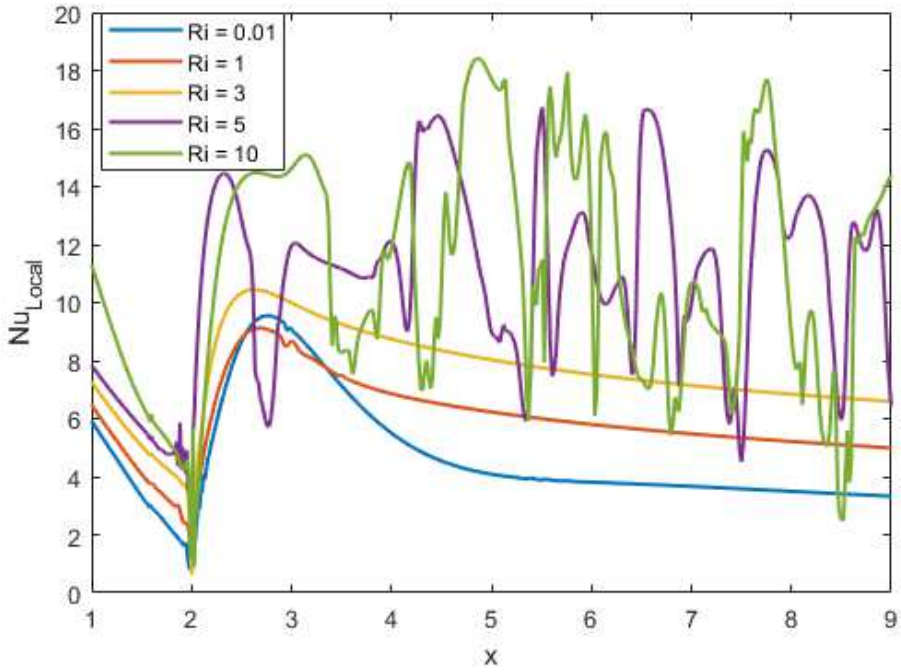
Local Nusselt Number

The local Nusselt number (Nu_{local}) changes with Richardson numbers ($Re = 0.01 - 10$), at $Re = 600$ and $\phi = 45°$ as shown in Fig. 11. The local Nusselt number distribution across the upper wall is presented for different Richardson numbers in the Fig. 11a at the same Reynolds number of $Re = 600$ and the same inclination angle of $\phi = 45°$. Since the forced convection is dominant and the buoyancy effect is small, Nu_{local} is smooth for $Ri = 0.01$. As buoyancy approaches the level of the inertial effects at $Ri = 1$, discernable differences occur. With $Ri = 3$ and 5 stronger peaks and fluctuations are seen as a result of the increased buoyancy-driven motion and local modification of the thermal boundary layer. The curve at $Ri = 10$ shows very strong fluctuations with sharp peaks, suggesting very high buoyancy effects and increased local mixing. In general, as Ri increases the flow and thermal field becomes more and more sensitive to buoyancy, and the variations of Nu_{local} become increasingly irregular.

The local Nusselt number is plotted across the lower wall for different Richardson number at $Re = 600$ and $\phi = 45°$ as shown in Fig. 11b. When $Ri = 0.01$, a decrease in Nu_{local} is noticed first and then slowly diminishes downstream due to the formation of the thermal boundary layer. The interaction between buoyancy and forced convection is greater near the bend, causing a noticeable increase in the value of $Ri = 1$. Enhanced buoyancy-driven motion and changes in the thermal boundary layer are seen for $Ri = 3$ and 5 with larger peaks and fluctuations. When $Ri = 10$, the fluctuations increase in intensity, showing several sharp fluctuations due to high buoyancy effects and increased mixing. In general, the higher Ri is, the greater the fluctuations in Nu_{local} will be, as the buoyancy will have more influence on the flow and thermal fields.



(a) Upper wall local Nusselt number for $Ri = 0.01, 1, 3, 5$ and 10.

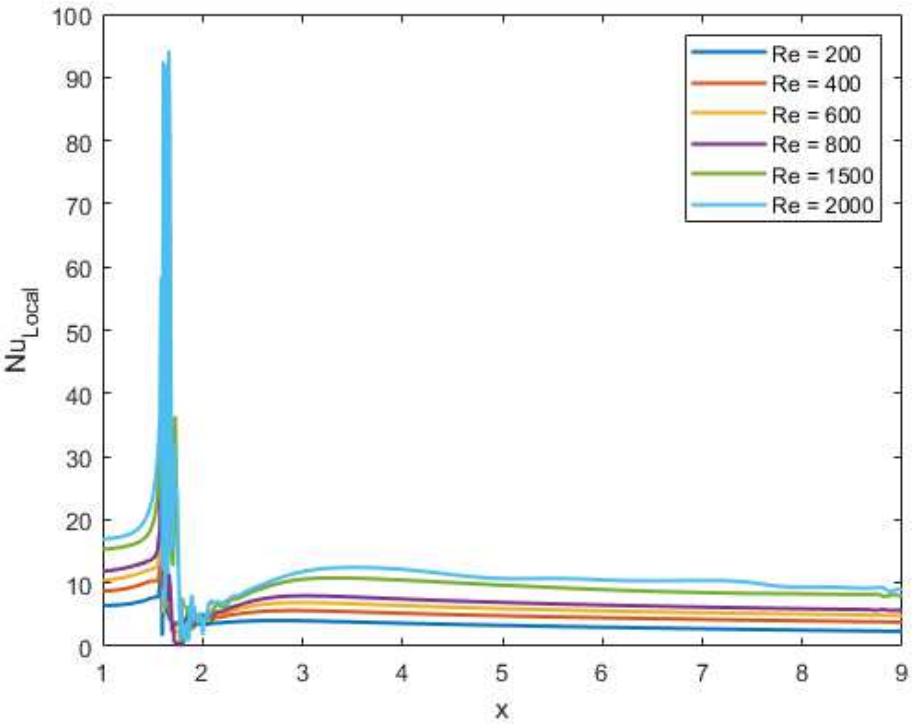


(b) Lower wall local Nusselt number for $Ri = 0.01, 1, 3, 5$ and 10.

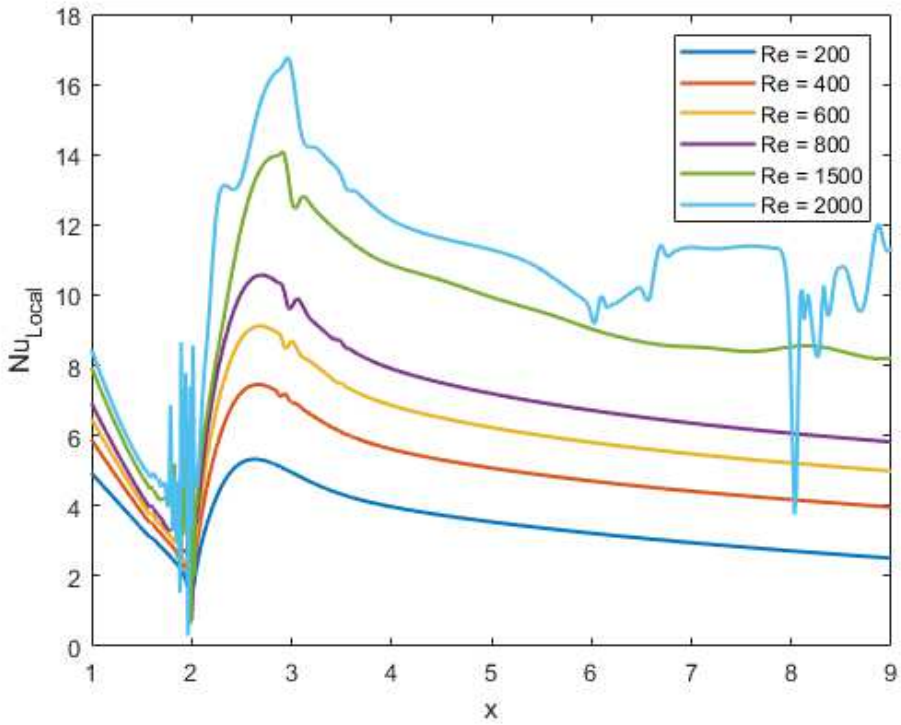
Figure 11: The impact of Richardson number variations on local Nusselt number is explored under the conditions $Re = 600$ and $\phi = 45°$

The local Nusselt number (Nu_{local}) changes with Reynolds number $Re = 200$ to 2000, at $Ri = 1$ and $\phi = 45°$ as shown in Fig. 12. The effect of local Nusselt number between the upper wall as illustrated in Fig. 12a. The downstream for $Re = 200$ the relatively low local Nu is caused by the weak fluid motion which restricts convective transport of the heat. Both local Nusselt numbers at $Re = 400$, 600 increase with stronger convection which improves heat transfer from the wall. A higher peak can be seen near the bend when $Re = 800$ as a result of the increased inertial effects and the disturbance of the thermal boundary layer. At $Re = 1500$ and 2000 a very sharp peak can be seen at the bend, followed by a higher Nu_{local} downstream, due to stronger mixing caused by the increased velocity of flow and the thinner thermal boundary layer. Therefore, the heat transfer coefficient increases generally with Re and the larger differences are found at the bend.

In Fig. 12b, the lower-wall Nu_{local} is still relatively low for $Re = 200$ due to the low velocity of the flow. The higher peaks at $Re = 400$ and $Re = 600$ are caused by the higher flow momentum that results in increased heat transfer. The greater the inertial forces, the more pronounced the peak becomes, which occurs at $Re = 800$. The peak is much higher at Re=1500, and the boundary layer is reestablished as the flow goes downstream. In the case of $Re = 2000$ the large convection creates intense mixing and a thin thermal boundary layer, which results in the highest Nu_{local}. The downstream fluctuations at high Re are related to the fluctuation of local flow and thermal field around the inclined section.



(a) Upper wall local Nusselt number for $Re = 200, 400, 600, 800, 1500$ and 2000.

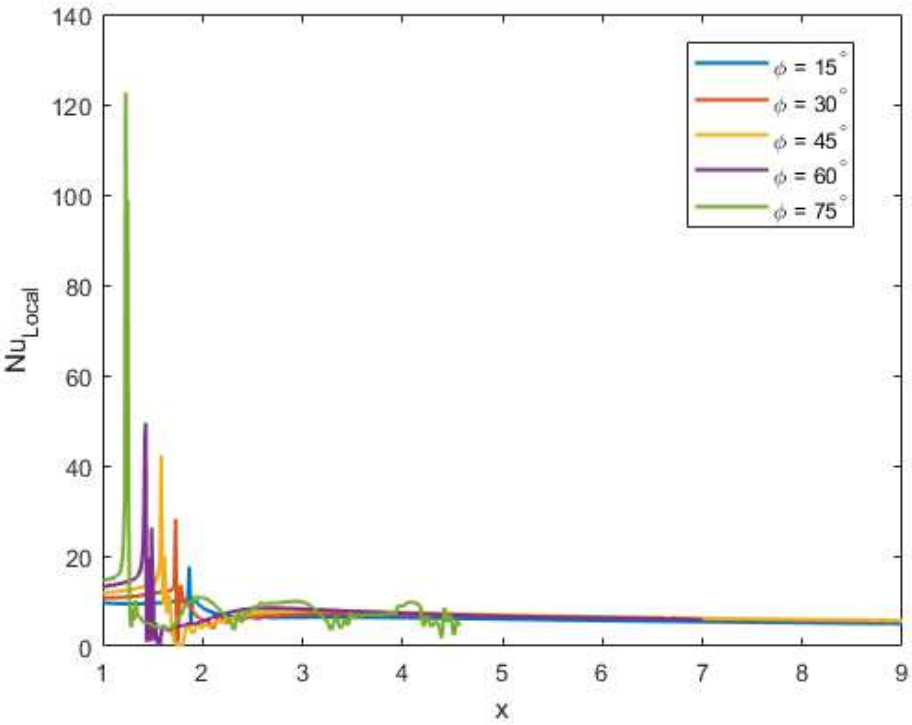


(b) Lower wall local Nusselt number for $Re = 200, 400, 600, 800, 1500$ and 2000.

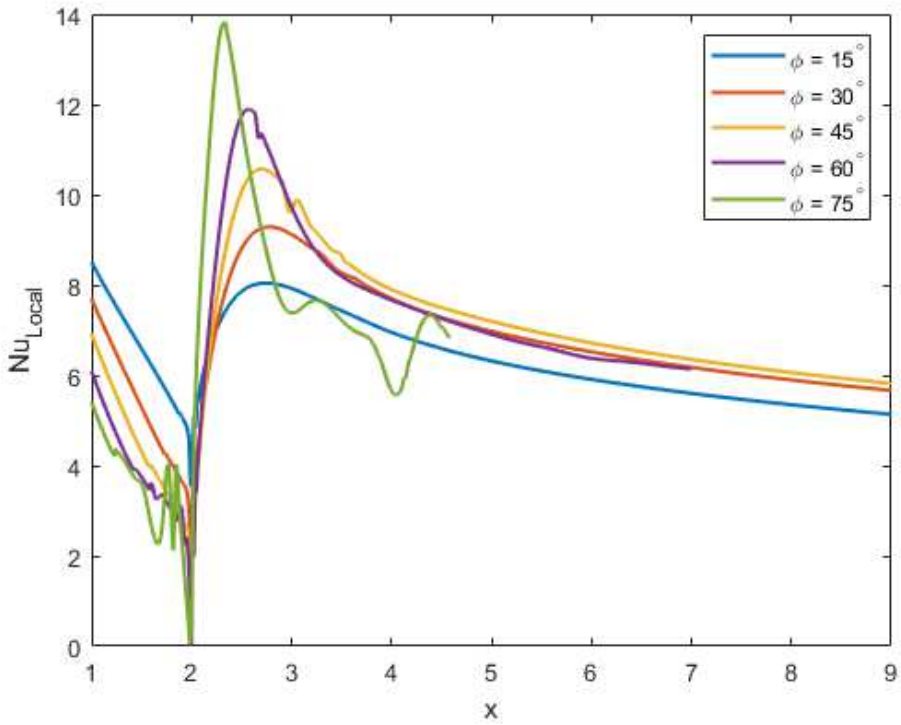
Figure 12: The impact of Reynolds number variations on local Nusselt number is explored under the conditions $Ri = 1$ and $\phi = 45°$

The variation of the inclination angle $\phi = 15°$–$75°$ on the local Nusselt number is shown in Fig. 13 for the case of $Ri = 1$ and $Re = 800$. The variation of the local Nusselt number through the upper wall shown in Fig. 13a. When $\phi = 15°$ the value of Nu_{local} has relatively small fluctuations since the component of the gravitational force along the pipe is small. The thermal boundary layer's profiles at $\phi = 30°$ and $45°$ show sharper peaks near the bend due to the enhanced buoyancy-driven flow as a result of the higher inclination angle. At $\phi = 60°$, stronger fluctuations are seen as there is an increased component of gravity along the inclined section. The maximum peak is located near the bend at $\phi = 75°$ as the maximum buoyancy-induced motion is generated at this location, causing larger local thermal mixing. The curves tend to become more alike further downstream as the flow and thermal fields re-develop.

The effect of the local Nusselt number for the lower wall is also presented in Fig. 13b for different inclination angles. The local Nusselt number decreases initially before a sharp rise after the bend for $\phi = 15°$; and the maximum is lower in comparison, caused by the low buoyancy effect. Higher peaks occur around the bend at $\phi = 30°$ and $45°$ where the buoyancy-driven heat transport is accelerated with the increase of the gravitational component. At $\phi = 60°$ buoyancy is stronger and flow is more re-distributed near the bend making the peak more pronounced. The maximum gravitational component along the pipe is at $\phi = 75°$ and therefore, the maximum buoyancy-driven motion and thermal mixing is observed at this value. Below the bend, Nu_{local} slowly decreases as the thermal boundary layer is reestablished.



(a) Upper wall local Nusselt number for $\phi = 15°, 30°, 45°, 60°$ and $75°$.



(b) Lower wall local Nusselt number for $\phi = 15°, 30°, 45°, 60°$ and $75°$.

Figure 13: The influence of ϕ variations on local Nusselt number is investigated under the conditions $Ri = 1$ and $Re = 800$.

The minimum, maximum and average values of the Nusselt numbers for various values of the Reynolds number, Richardson number and inclination angle are summarized in the Table 2. The results indicate that the three parameters have significant impact on the heat-transfer performance. The general trend is that with increasing Re from 200 to 2000 for $Ri = 1$ and $\phi = 45°$ the maximum and average Nusselt numbers for both walls increases. This is because greater Re makes inertial effects and convective mixing more pronounced which decreases the thickness of the thermal boundary layer and thus increases the temperature gradient across the wall.

The Nusselt number increases with the increase of Ri from 0.01 to 10 at $Re = 600$ and $\phi = 45°$ in general, because of the intensified buoyancy-driven flow. The secondary flow creates turbulence in the thermal boundary layer and enhances heat transport. For $Re = 800$ and $Ri = 1$, the maximum Nusselt number increases considerably as ϕ increases from 15° to 75° especially at the upper wall. This is because a greater inclination enhances gravity driven flow along the pipe, which boosts buoyancy driven flow and local thermal mixing. Generally heating due to convective heat transfer increases with increasing Re, Ri, and increasing ϕ.

Table 2: Variation of Nusselt number at different walls.

Re	Ri	ϕ	Upper Wall			Lower Wall		
			Nu_{min}	Nu_{max}	Nu_{avg}	Nu_{min}	Nu_{max}	Nu_{avg}
200	1	45°	1.64	24.90	3.97	0.75	9.17	3.73
400	1	45°	2.91	33.99	5.56	0.87	11.32	5.12
	0.01	45°	0.05	37.49	5.06	0.68	12.25	4.93
	1	45°	1.81	38.74	6.69	0.94	12.79	6.14
600	3	45°	0.43	40.54	8.41	0.62	13.60	7.62
	5	45°	0.20	41.63	9.28	2.09	16.73	10.40
	10	45°	0.07	49.88	9.87	0.88	18.90	11.14
	1	15°	4.59	17.62	6.49	3.53	13.52	6.31
	1	30°	1.04	28.15	7.19	1.74	13.52	6.71
800	1	45°	0.02	42.35	7.61	0.98	13.91	6.97
	1	60°	0.15	49.51	8.54	0.03	15.02	7.08
	1	75°	1.79	122.62	9.74	0.04	16.98	7.14
1500	1	45°	0.69	62.82	10.78	0.63	16.51	9.10
2000	1	45°	0.72	94.20	12.45	0.30	17.63	10.60

4 Conclusion

This paper deals with the numerical study of the mixed convective fluid flow and heat transfer phenomena in a bent pipe with various inclined angles by Finite Difference Method (FDM) in MATLAB. The flow field, temperature field and local heat transfer were examined in terms of the streamline, isotherm and local Nusselt number distributions and the effect of Richardson number (Ri), Reynolds number (Re) and inclination angle (ϕ) were examined. The key findings are summarized below:

1. As the Re value increases from 200 to 2000, the convective heat transfer will increase, increasing the Nu_{avg} value by 213.6% on the upper wall and 184.2% on the lower wall.

2. The average heat transfer rate increases by 95.1% and 25.9% on the upper and lower surfaces, respectively, for an increase in the buoyancy parameter (Ri from 0.01 to 10) at fixed $Re = 600$.

3. At $Re = 800$, the inclination angle ϕ is changed from 15° to 75°, the upper wall heat transfer increases significantly by 50.1%, and the lower wall heat transfer is relatively stable, with a small increase of 13.2%.

In summary, it can be seen that the Reynolds number, Richardson number and the inclination angle have significant effects on the flow and thermal field in the bent pipe. The higher the values of these parameters, the higher the convective heat transfer, because they increase the fluid mixing and the temperature differences from the wall. The results are helpful for the thermal design of systems containing curved or inclined flow passages.

Declaration of competing interest: The authors indicate that they have no conflict of interest.

Data availability: Data will be made available on a valid request to the corresponding author.

Funding: The authors received no specific funding for this work.

References

[1] Shahsavar, A., Entezari, S., Toghraie, D., & Barnoon, P. (2020). Effects of the porous medium and water-silver biological nanofluid on the performance of a newly designed heat sink by using first and second laws of thermodynamics. *Chinese Journal of Chemical Engineering, 2*8(11), 2928-2937.

[2] Hickie-Bentzen, A., Elsharqawy, M., Tasnim, S. H., & Mahmud, S. (2022). Parametric investigation of internal Y-shaped fin configurations under natural convection in a concentric annulus. Results in Engineering, 16, 100692.

[3] Lauriat, G., & Ghafir, R. (2000). Forced convective heat transfer in porous media. *Handbook of Porous Media*, 201-204.

[4] Carmeliet, J., Descamps, F., & Houvenaghel, G. (1999). A multiscale network model for simulating moisture transfer properties of porous media. *Transport in porous media, 35*(1), 67-88.

[5] A.T. Prata and E.M. Sparrow, "Heat transfer and fluid flow characteristics for an annulus of periodically varying cross section," *Numerical Heat Transfer*, vol. 7, no. 3, pp. 285–304, 1984, Taylor & Francis.

[6] S.V. Patankar, C.H. Liu, and E.M. Sparrow, "Fully developed flow and heat transfer in ducts having streamwise-periodic variations of cross-sectional area," *Journal of Heat Transfer*, vol. 99, no. 2, pp. 180–186, 1977.

[7] M. A. Merrigan, E. S. Keddy, J. T. Sena, and M. G. Elder, "Heat pipe technology development for high temperature space radiator applications," *Los Alamos Nat. Lab. (LANL)*, Los Alamos, NM, USA, Tech. Rep., 1984.

[8] N. Acharya, M. Sen, and H.-C. Chang, "Heat transfer enhancement in coiled tubes by chaotic mixing," *Int. J. Heat Mass Transf.*, vol. 35, no. 10, pp. 2475–2489, 1992.

[9] M. Ouzzane, and N. Galanis "Numerical Analysis Of Mixed Convection In Inclined Tubes With External Longitudinal Fins" *Solar Energy.*, vol. 71, no. 1–3, pp. 199–211, 2001.

[10] Y. Chuanyong, X.Jinliang and W. Xiaodong "Mixed convective flow and heat transfer of supercritical CO2 in circular tubes at various inclination angles " *International Journal of Heat and Mass Transfer.*, vol. 64, no. 1–3, pp. 212–223.

[11] L.Chin, and C.Yun, "Numerical Study on Mixed Convection Heat Transfer in Inclined Triangular Cavities" *Numerical Heat Transfer*, vol. 67, 2015.

[12] C.Huajun, and Z.Benzhao, "Fluid flow and mixed convection heat transfer in a rotating curved pipe," *International Journal of Thermal Sciences*, vol. 42, pp. 1047–1059, 2017.

[13] J. Chen, P. Yu, Z. F. Tian, and H. Ouyang, "A Higher-Order Compact Scheme for Solving the 2D Steady Incompressible Navier–Stokes Equations in General Curvilinear Coordinates," *International Journal of Numerical Methods for Heat & Fluid Flow*, vol. 32, no. 5, pp. 456–477, 2020.

[14] Chen J, Yu P, Tian ZF, Ouyang H. A high-order compact scheme for solving the 2D steady incompressible Navier-Stokes equations in general curvilinear coordinates. Numerical Methods in Fluids. 2019;92(5):456–77.

[15] Matsumoto, D., Fukudome, K., & Wada, H. (2016). Two-dimensional fluid dynamics in a sharply bent channel: Laminar flow, separation bubble, and vortex dynamics. *Physics of Fluids, 28*(10).

[16] Nithiarasu, P., Seetharamu, K. N., & Sundararajan, T. (1997). Natural convective heat transfer in a fluid saturated variable porosity medium. *International Journal of Heat and Mass Transfer, 40*(16), 3955-3967.